Check for updates

An update on recent advances in fluorescent materials for fluorescence molecular imaging: a review

Nkune Williams Nkune, [ID] Kave Moloudi, Blassan P. George [ID] and Heidi Abrahamse [ID] *

Fluorescence molecular imaging (FMI) is a powerful imaging technique used primarily in biomedical research and clinical applications to visualize molecular and cellular processes of tumors and other diseases. FMI involves the use of fluorescent molecules (fluorophores) that absorb light at one wavelength and emit it at a longer wavelength. These fluorophores can be attached to specific molecules and markers (such as proteins, nucleic acids, or small molecules) in a biological sample. FMI typically offers non-radioactive and safe, real-time and higher spatial resolution compared to positron emission tomography (PET) for superficial tumors. Additionally, sensitivity and specificity of FMI for superficial tumors in better than PET is some cases. However, FMI and the materials used in molecular imaging (MI) have revolutionized biomedical research, diagnostics, and therapeutic monitoring. In contrast, despite their significant contributions, several challenges remain to be solved to improve the effective application of fluorescence-based techniques. These challenges are related to poor tissue penetration depth, background autofluorescence, photobleaching of fluorophores, low signal-to-noise ratio in deep tissues and the necessity for biocompatible and photostable probes. Hence, ongoing improvements in probe development, imaging technologies and analytical methods are required to overcome current challenges. Future advancements in fluorescence materials and imaging techniques hold promise for making MI more accurate, efficient and applicable for clinical and research scenarios. This review gives an overview of recent advances in the materials used in MI and findings of FMI. Finally, limitations of FMI are highlighted and recommendations for future research directions are proposed.

1. Introduction

Molecular imaging (MI) is a state-of-the-art field of science that can be used for cancer diagnosis and treatment monitoring, cardiovascular research, neurological studies, drug development and gene therapy and cell tracking.[1,2] Various kinds of MI techniques, including positron emission tomography (PET), single-photon emission computed tomography (SPECT), magnetic resonance imaging (MRI), functional MRI (fMRI) and fluorescence imaging (FI) are often combined with PET (PET/CT, PET/MRI) to provide both anatomical and functional information. MI utilizes radioisotopes and fluorescent probes to detect cancer cells, disease and specific cells or molecules and can be applied *in vitro*, *in vivo* and at the clinical level.[3,4]

Fluorescence in MI is a powerful technique used to visualize and study biological processes at the molecular level. This method relies on the emission of light by a substance that has absorbed light or other electromagnetic radiation. Principles of fluorescence are utilized in MI based on excitation and

emission; when a fluorophore (a fluorescent molecule) absorbs photons, it becomes excited and subsequently emits light at a longer wavelength as it returns to its ground state. These principles are based on Shimomura's purification of green fluorescent protein (GFP) from Aequorea victoria jelly, which gained him recognition.[5] The engineering of GTP for mammalian expression in biochemistry and cell biology applications has revolutionised the field of live-cell imaging and studies have advanced fluorescence resonance energy transfer (FRET) to prominence as the primary foundation for molecular interaction studies.[5–7]

The light emission of the photoexcited fluorophore in MI can be detected and used for imaging.[8,9] Thereare the various types of natural (like GFP) or synthesized molecules and dyes that can be used in fluorescence imaging. The choice of fluorophore depends on factors like brightness, stability, and the specific wavelength required for the application. Moreover, some materials work based on the Stokes shift phenomenon, which is the difference in wavelength between the absorbed light and emitted light. It allows for the separation of excitation and emission signals, which is crucial for clear imaging.[10,11]

Laser Research Centre, Faculty of Health Sciences, Doornfontein Campus, University of Johannesburg, Johannesburg, 2028, South Africa. E-mail: habrahamse@uj.ac.za

MI can be employed for cellular imaging, quantitative analysis (measuring the concentration of specific molecules), multimodal imaging (such as magnetic resonance imaging (MRI) or positron emission tomography (PET)) and FRET; this technique allows for the study of interactions between biomolecules. Even though some advantages of FI include high sensitivity, real-time imaging and specificity that specific proteins or structures can be visualized. But there are still some challenges to be addressed, such as background noise, depth penetration and photobleaching, where fluorophores can lose their ability to fluoresce over time when exposed to light.[12,13] Molecular imaging is a rapidly evolving field that bridges the gap between molecular biology and imaging technologies. It holds great promise for advancing our understanding of biological processes, improving disease diagnosis, and guiding therapeutic interventions. As technology continues to advance, molecular imaging is expected to play an increasingly critical role in personalized medicine and translational research. However, in this review, the latest findings and challenges of fluorescence imaging and materials in FI are highlighted.

2. Various kinds of radioisotopes, materials and antibodies in molecular imaging (MI)

In FMI, various materials and antibodies are utilized to visualize and quantify biological processes at the molecular level. These materials and antibodies can be broadly categorized based on their function, specificity and application in imaging techniques.[14,15] Various types of common materials and antibodies for MI applications are overviewed in Table 1. The choice of materials depends on the specific application, desired sensitivity, resolution and the biological targets involved.[16,17] The first class of materials are fluorescent dyes and probes that can be employed in FI *via* emitting fluorescence upon excitation by specific wavelengths of light. The common agents and probes include fluorescein isothiocyanate (FITC), rhodamine, cyanine 3 (CY3) and 5 (Cy5), Alexa Fluor dyes, indocyanine green (ICG), ion indicator probes and pH indicators that are used in pathology and cancerous tissues for real-time imaging under microscope.[1,18,19] The second class of materials that are used for FI are antibodies such as trastuzumab (Herceptin), polyclonal antibodies, Fab fragments and nanobodies for visualizing specific proteins or antigens in biological samples. Antibodies derived from a single clone of B cells, providing high specificity for a single epitope (receptor) or recognizing multiple epitopes.[20] For instance, trastuzumab can be conjugated to fluorescent dyes (*e.g.*, FITC, Alexa Fluor) to visualize human epidermal growth factor receptor-positive 2 (HER2) tumors *in vivo* or *ex vivo*.[21,22] Moreover, polyclonal antibodies are derived from multiple B-cell lineages and can recognize multiple epitopes on a single antigen.[23] Another example is Fab fragments, which are the antigen-binding portions of antibodies, produced by enzymatic cleavage of whole antibodies. They retain the ability to bind to their specific antigens but lack the Fc region.[24] The third class of materials based on light and fluorescence imaging (FI) consists of contrast agents or fluorescent dyes that can be used alongside optical coherence tomography (OCT) to enhance the visualization of specific superficial tissues, microvascular structures, angiography, tumors, or inflammation. Examples of this category include ICG, exogenous dyes such as methylene blue and Evans blue, fluorescein sodium, avidin-biotin complexes, and nanoparticles like gold nanoparticles (AuNPs) and silica.[25–28]

Various contrast agents and fluorescent dyes enhance the imaging capabilities in different kinds of imaging techniques by increasing tissue contrast, highlighting specific structures and providing more detailed visualization, especially in areas like ophthalmology, oncology, and cardiovascular diagnostics.

Table 1 Some key materials and antibodies commonly used in various FI[a]

Category	Types of materials	Function	Types of techniques of MI	References
1	Fluorescent dyes and probes: fluorescein isothiocyanate (FITC), rhodamine, Cy3 and Cy5, Alexa Fluor dyes, indocyanine green (ICG)	Emitting fluorescence upon excitation by specific wavelengths of light	FI	20–22
2	Antibodies: Trastuzumab (Herceptin), polyclonal antibodies, Fab fragments, nanobodies	Antibodies derived from a single clone of B cells, providing high specificity for a single epitope (receptor) or recognize multiple epitopes	FI	23 and 24
3	Contrast agents for OCT: ICG, exogenous dyes (methyleneblue, evans blue) fluorescein sodium, avidin-biotin complexes and nanoparticles (AuNPs and silica)	Designed for fluorescence imaging, often incorporating both a targeting ligand and a fluorescent dye	OCT (FI)	25–28

[a] FI, fluorescence imaging; OCT, optical coherence tomography; Cy5, cyanine 5; ICG, indocyanine green; AuNPs, gold nanoparticles.

3. Principle of fluorescence molecular imaging (FMI)

FMI relies on the principles of fluorescence, where certain molecules (fluorophores) absorb light at specific wavelengths and emit light at longer wavelengths. However, as can be seen in Fig. 1, the photophysical process involves the absorption and re-emission of light. A fluorophore absorbs a photon of light (usually ultraviolet or blue light) and excites the fluorophore's electrons to a higher energy state (excited state). Consequently, the excited electron quickly relaxes to a lower energy level (within the excited state), releasing some energy as heat. This is called non-irradiative relaxation. After the relaxation step, the fluorophore returns to its ground state by emitting a photon at a longer wavelength than the excitation wavelength, resulting in this emitted light being detected in FI. Additionally, emitted light for fluorescent agents has some properties, such as the Stokes shift (the difference between the excitation and emission wavelengths), fluorescence lifetime and quantum yield that could affect the imaging process. Therefore, besides the source of emission light and fluorescence material features, biological properties of the cells and tissue and imaging facilities (resolution and real-time) are important during FI.[29–31]

To achieve high-quality fluorescence imaging, certain essential facilities and equipment are required, including a fluorescence microscope or confocal microscope, a fluorescence light source (*e.g.*, laser), fluorophores (*e.g.*, dyes or probes), detectors, optical filters and dichroic mirrors, and image processing and analysis software (*e.g.*, ImageJ, MATLAB).[14,32,33]

4. Specific fluorescence dyes and materials in fluorescence molecular imaging

The choice of fluorescent dyes and materials in molecular imaging depends on the specific application, including the type of biological sample, the desired resolution, sensitivity, and the nature of the targets being studied. Despite traditional dyes such as FITC and Cy-series being widely used, BODIPY (boron-dipyrromethene) dyes have shown great promise as versatile fluorescent probes in cellular imaging and therapeutic applications due to their exceptional chemical properties, such as remarkable fluorescence quantum yields (>0.8), strong extinction coefficients, exceptional photostability and tunable emission (500–700 nm) *via* structural adjustments.[34] Recent studies have focused on developing novel BODIPYs modified with targeting moieties such as folic acid (folate-conjugated BODIPY) for targeted cancer imaging to promote tumour-specific uptake, organelle imaging (mitochondrial/lysosomal tracking), and NIR imaging (>1000 nm) for improved tissue penetration depth. In addition, BODIPYs allow for dual imaging and photodynamic therapy, demonstrating their multifunctional applications[35–39].

Studies by Jurgutis *et al.* investigate the ability to detect the microviscosity of biological objects using the BODIPY-based molecular BDP-H, a water-compatible probe ideal for live-cell imaging of intracellular microviscosity in human breast cancer cells. Jurgutis and colleagues noted that BDP-H permeated through the plasma membrane and localised primarily in lipid droplets (LDs), which allowed for viscosity measurements
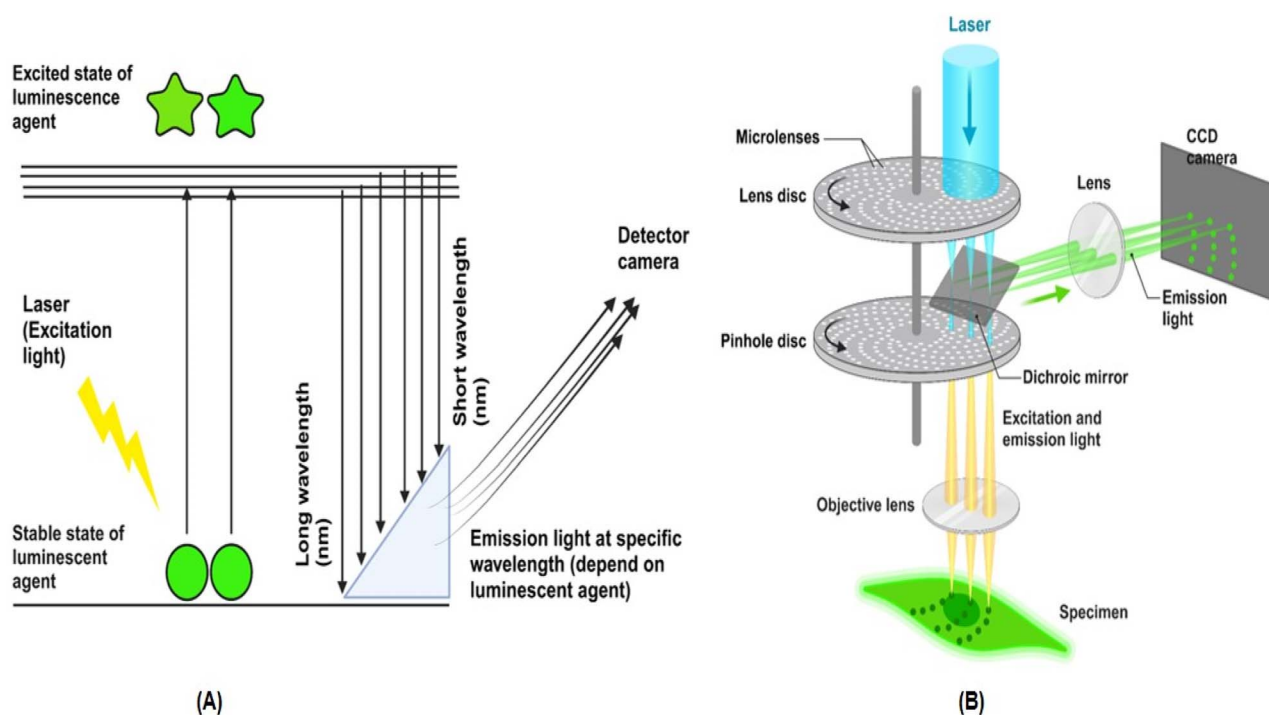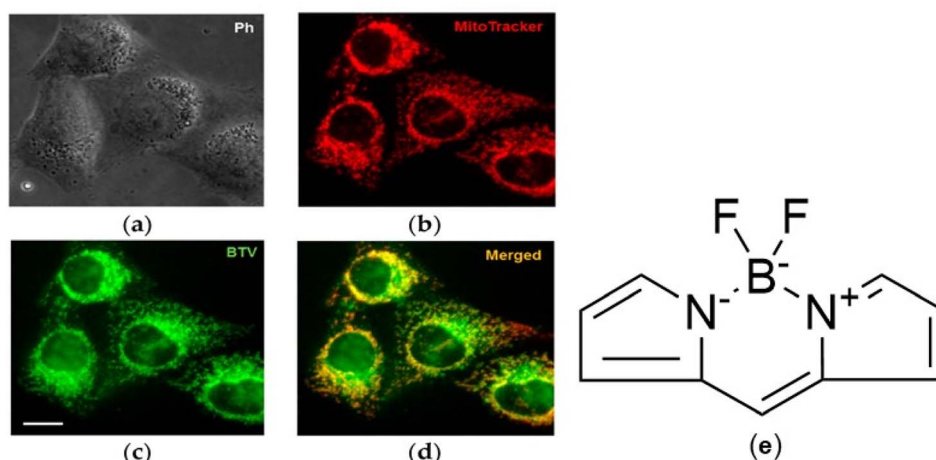

Fig. 1 Principal of FI using luminescence agent such as green fluorescence probe (GFP) and confocal microscopy. (A), a schematic of principles of FMI, (B), fluorescence confocal microscopy and various stages of FI and recording image from sample.

Fig. 2 Fluorescence microscopic images of BODIPY-based viscosity probe (BTV) in HeLa cells with stained with MitoTracker. DeepRed. Images were taken with a 40× objective. Scale bar represents 20 μm. (a) Phase contrast; (b) MitoTracker DeepRed; (c) BTV; (d) merged of MitoTracker DeepRed and BTV. Adapted from ref. 65 (under the terms of the Creative Commons CC BY 4.0 license (e) chemical structure of BODIPY dye.

using fluorescence lifetime imaging microscopy (FLIM). Jurgutis and colleagues noted that BDP-H permeated through the plasma membrane and localised primarily in lipid droplets (LDs), which allowed for viscosity measurements using fluorescence lifetime imaging microscopy (FLIM). On further analysis, FLIM results reported that microviscosity in LDs of aggressive breast cancer cells (MDA-MB-231 cells) was significantly higher than in MCF-7, indicating that LD microviscosity could be used as a biomarker for cancer cell malignancy. However, BDP-NO$_2$ agglomerated in aqueous conditions, showing inadequacy for live cell applications.[40] The capability of BODIPY-based probes to visualize intracellular viscosity if further demonstrated in live-cell imaging studies, shown in Fig. 2.

NIR dyes such as indocyanine green (ICG) have been widely used in biomedical research such as sentinel lymph node (the first station of lymph node for malignant tumour drainage) biopsy, tumour locating, imaging-guided surgery procedures, determination of resection margins, lymph node fluorescence harvesting, and anastomotic perfusion assessment; however, they lack target specificity.[41,42] This has led to the development of novel NIR dyes such as IR-780 and MHI-148, which have shown remarkable target selectivity and negligible off-target toxicity.[43] Recent studies by Luo et al. developed an NIR fluorescent probe, 4-(2-(4-(dicyanomethylene)-4H-chromen-2-yl)vinyl)phenyl 2,3,4,5,6-pentafluorobenzenesulfonate (DCM-H$_2$O$_2$) probe, to detect hydrogen peroxide (H$_2$O$_2$) in living cells and scald and incision wound mice models.[44] Research indicates that H$_2$O$_2$ activates various biological pathways which promote wounding healing. Lou and colleagues reported that DCM-H$_2$O$_2$ demonstrated a low detection limit and high specificity with low cytotoxicity for H$_2$O$_2$, making it suitable for in vivo application. The probe effectively monitored variations of endogenous H$_2$O$_2$ during proliferation process of human immortalized epidermal (HACAT) cells, suggesting that H$_2$O$_2$ plays a key in cellular proliferation through a growth factor

signaling pathway. In vivo fluorescence signals were successfully detected in the scald and incision wound mice models, enabling the measurement of H$_2$O$_2$ concentration variations at different pathological stages during the wound healing process. Furthermore, the probe also monitored H$_2$O$_2$ concentrations in different stages of human diabetic foot tissues. Luo and colleagues concluded that their novel NIR probe confirmed that H$_2$O$_2$ could be a reliable biomarker for monitoring the wound healing process.

Another recent study conducted by Luo synthesised an NIR two-photon fluorescent probe (HDM-Cl-HClO to detect variations in hypochlorous acid (HClO), an essential biomolecule in living organisms which facilitate various physiological or pathological mechanisms. Elevated levels of HClO promote inflammation and malignancies. Thus, Lou and colleagues design the HDM-Cl-HClO probe to assess variations in HClO levels in inflammatory and tumor-bearing mice. The probe showed a prompt response to HClO within 5 seconds and elicited a strong red fluorescence at 660 nm indicative of high specificity and sensitivity for HClO. The excellent spectral capability of the probe not only allowed for the detection of HClO levels in cells and zebrafish but also detected HClO in inflammatory and tumor mice. This study not only introduced a novel approach for imaging HClO in living systems, but also holds great promise for the diagnosis of inflammatory diseases and cancers.[45]

Xia et al. investigated the cytotoxic, in vivo imaging of MHI-148 in lung-cancer nude mice model. Ex vivo imaging was also been measured by testing the major tissue fluorescence intensity. And, the small molecular compound MHI-148 exhibited insignificant cytotoxicity which could be visualized at 1 h post-injection in tumor. From ex vivo fluorescence imaging, the tumor demonstrated the maximum uptake of MHI-148 among all the selected organs expect for the time point of 2 h. MHI-148 could be used for effective imaging in lung cancer tissue with good stability and specificity, which
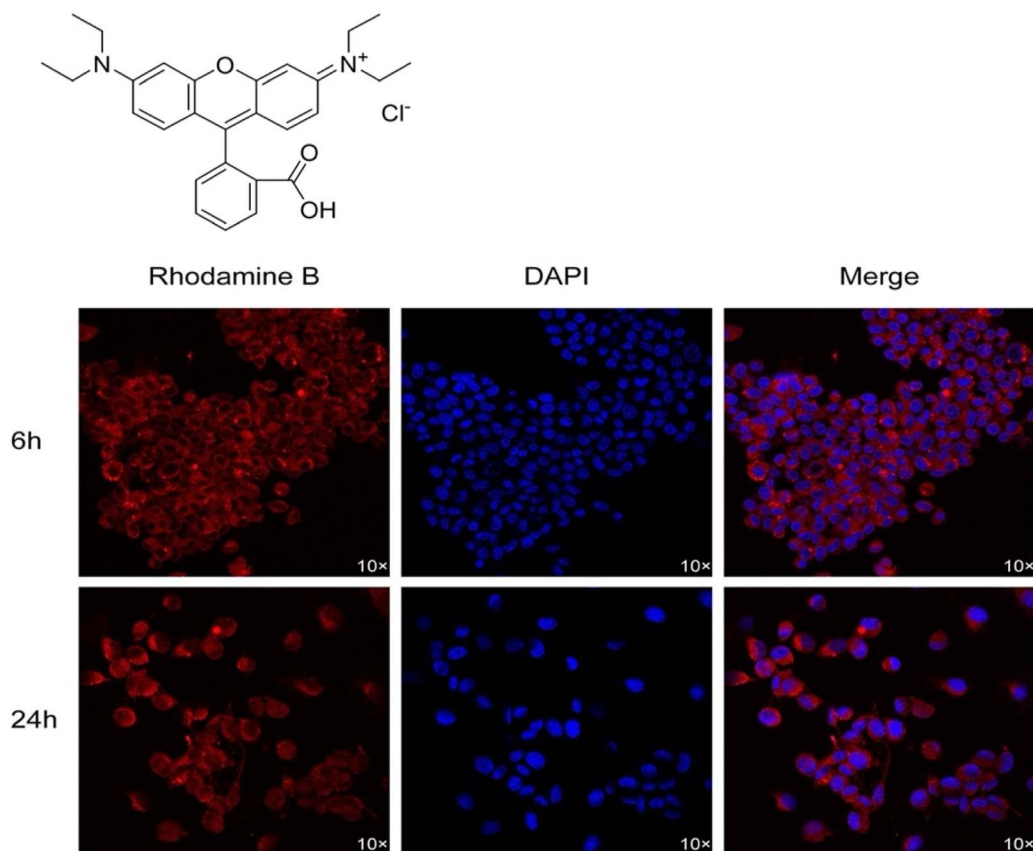
Fig. 3 Fluorescence microscopy image of neuronal cells (ND7/23) incubated with Rhodamine B. Adapted from ref. 109, under the terms of the Creative Commons CC BY 4.0 license.

suggested that MHI-148 has a potential to be an effective tumor clinical imaging agent.[46] Upconversion of light has gained popularity in biomedical research due to its ability to analysed deep-seated tissue, owing to the longer wavelength of incident light compared to downconversion fluorescent materials.

Upconversion materials based on triplet–triplet annihilation (TTA) exhibit low excitation power (*e.g.*, ambient sunlight) and ease of tunable excitation and emission wavelengths. TTA-based delayed fluorescence probes yield background-free imaging. These systems rely on sensitiser-acceptor pairs to convert low-energy excitation light into higher-energy emission. This process not only allows for deep tissue imaging (beyond 5 mm) but also minimises autofluorescence interference with negligible photodamage.[47–51]

Advances in dye chemistry and nanotechnology continue to enhance the capabilities of molecular imaging, enabling more precise and informative studies in biology and medicine. Mai *et al.* (2022) developed lactose-functionalised BODIPY nanoparticles (NPs) which showed remarkable fluorescence imaging and phototoxicity against various cancer cell lines (HeLa and Huh-7 cells). The nanoconjugate exhibited high $^1O_2$ generation capability and ΦF to pave new avenues for useful imaging-guided PDT agents for tumour cells.[52] Vepris *et al.* investigated biodegradable poly (lactic-*co*-glycollic acid) (PLGA) nanoparticles as a nanocarrier system for triplet–triplet annihilation

upconversion (TTA-UC) based on the heavy metal porphyrin platinum(II) octaethylporphyrin (PtOEP) and the polycyclic aromatic hydrocarbon 9,10-diphenylanthracene (DPA) as a photosensitiser/emitter pair. TTA-UC-PLGA-NPs were successfully synthesised using an oil-in-water emulsion and solvent evaporation method. These TTA-UC-PLGA-NPs demonstrated a remarkable upconversion under low-power excitation, ideal for clinical applications. Physicochemical studies confirmed successful synthesis, and UC efficiency was investigated *in vitro* and *ex vivo*. More importantly, *in vivo* studies emitted TTA-UC signals in tumours 96 hours post-administration, demonstrating the NPs' stability and biocompatibility as an *in vivo* nanocarrier system. This study suggests that the synergistic effects of PLGA and TTA-AUC optical properties allow for simultaneous imaging and drug delivery.[53]

Quantum dots (QDs) offer essential advantages required in imaging due to their enhanced brightness, photostability and narrow emission spectra in comparison with organic dyes. These characteristics are very important for various applications such as bioimaging, diagnosis and delivery of therapeutics. Furthermore, QDs can also be modified with various targeting moieties and are suitable for multifunctional purposes, allowing for simultaneous detection of multiple targets.[54–56]

Table 2 Various types of specific fluorescence dyes and materials in MI have been summarized[a]

Types of materials	Excitation/emission wavelength	Photoluminescence quantum yield (PLQY)	Lifetime (ns) and condition	Characteristics	Applications	Ref.
Fluorescein isothiocyanate (FITC)	495 nm/519 nm	0.92	4–5 in 2 M NaOH	Bright green fluorescence, commonly used for labeling proteins and antibodies	Immunofluorescence, flow cytometry, and microscopy	66–68
Rhodamine B	540 nm/625 nm	0.65	2.72 in ethanol	Bright red fluorescence; high photostability	Cell tracking, immunofluorescence, and live-cell imaging (Fig. 3)	69–72
Cy3 and Cy5	Cy3: 550 nm/570 nm; Cy5: 650 nm/670 nm	0.15–0.16; 0.20–0.30	0.18 in water; 0.8–1.07 in water	Green and red emission	Cy3: often used in multiplexing experiments due to distinct spectral properties; Cy5: commonly used in combination with Cy3 for dual-labeling experiments	73–77
Alexa Fluor dyes	Fluor 488, Fluor 594, Fluor 647	0.1–0.3	1.0–4.1 in PBS	High brightness, photostability, and a wide range of colors	Suitable for various applications including immunofluorescence, live-cell imaging, and multiplex assays	78
Near-infrared (NIR) dyes: Indocyanine green (ICG)	800 nm/830 nm	0.2	1.66 in water	Emission NIR color	Used in clinical imaging for vascular studies and tumor detection due to low tissue absorption	59 and 79–81
BODIPY dyes	493 nm/503 nm	0.7–0.99	4–6 in water	High fluorescence quantum yield and photostability	Used in live-cell imaging and as probes for lipid detection	82–87
Quantum dots	300 nm to 500 nm/400 nm to 700 nm	—	10–40 in water	Semiconductor nanoparticles that exhibit size-tunable fluorescence	Used for multiplexing in imaging due to their broad absorption spectra and narrow emission spectra	88–90
DAPI (4',6-diamidino-2-phenylindole)	358 nm/461 nm	0.92	2.6–2.9 DNA bound	Binds strongly to DNA; emits blue fluorescence	Commonly used for nuclear staining in fixed cells	91 and 92
Propidium iodide (PI)	535 nm/617 nm	0.9	18.11 DNA bound	A DNA-binding dye that cannot permeate live cells; emits red fluorescence	Used for staining dead cells in flow cytometry	93–96
Nanoparticles: gold nanoparticles (AuNPs), silica nanoparticles	AuNPs: 520–580 nm/660 nm; Silica nanoparticles: 540 nm/580 nm	—; —	<1 ps in water; N/A	As nanotheranostics agents for various cancers	Can be functionalized with fluorescent dyes for imaging applications and can be modified for specific targeting	97–99
Fluorescent protein tags: GFP and its derivatives (e.g., mCherry, mKate)	GFP: 488 nm/509 nm; mCherry: 587 nm/610 nm; mKate: 588 nm/633 nm	0.72–0.85; 0.22; 0.28–0.33	2.3–3.5 at 37 °C; 1.4–1.6 pH 7.5; 1.45–1.55 pH 7.5	Genetically encoded fluorescent proteins that allow for real-time study gene expression and imaging of live cells	Used in transgenic models to study gene expression and protein localization	6 and 100–108

[a] NaOH, sodium hydroxide; NIR, near-infrared; ps, picosecond; PBS, phosphate-buffered saline; DNA, deoxyribonucleic acid; BODIPY, boron-dipyrromethene; GFP, green fluorescent protein; AuNPs, gold nanoparticles.

Various types of specific fluorescence dyes and materials in FI have been summarized in Table 2. All these fluorescent dyes and materials would be excited at specific wavelengths and then emit at specific wavelengths of light or different colours, consequently. Moreover, each fluorescent dye and material has its own characteristics and applications to visualize cells, DNA and proteins. In relation to emissions summarised in Table 2, the NIR window of 650–980 nm is the most feasible range for imaging diseases tissues. NIR is has shown low light scattering and tissue autofluorescence, which enhances the signal-to-noise ratio and the resolution of imaging.[57,58] NIR fluorescent dyes such as ICG and IR-780 iodide have garnered considerable interest imaging animal and human tissues due to their improved tissue penetration depth.[59,60] The best solvents for dissolving the aforementioned fluorophores are dimethyl sulfoxide (DMSO), ethanol, and phosphate-buffered saline (PBS) due to their ability to ensure stability and dissolve hydrophobic compounds. Thus, selecting an appropriate solvent takes precedence as it affects the photostability, cellular uptake and biocompatibility of fluorophores, all of which are indispensable to imaging success.[61–64]

5. FMI *in vitro, in vivo* and clinical studies

FMI is a powerful technique used to detect and quantify biological processes for various diseases at the molecular and cellular levels *in vitro*, *in vivo* and in clinical contexts (Table 3). Fluorescent markers can be labelled to specific proteins, organelles or cellular structures, allowing the visualization of cellular processes like apoptosis, proliferation or migration. Moreover, fluorescent assays are employed to evaluate the efficacy of drugs on cultured cells, protein–protein interactions, biodistribution of nanoparticles, gene expression studies and monitoring changes in fluorescence intensity or localization. A recent study by Luo *et al.* developed a dual-channel fluorescent probe for precise identification of senescent cells *via* simultaneous detection of b-galactosidase (b-gal) and a-L-fucosidase (AFU), two biomarker markers that are elevated in senescent cells. Luo and co-workers successfully designed a fluorescent probe HDQ-NA-AFUGal for precise imaging of cellular senescence associated with b-gal and AFU enzymes. The presence of b-gal and AFU was confirmed by this dual-response fluorescent, which emitted strong fluorescence signals at 740 nm (red) and 550 nm (green), respectively, enabling definite identification of b-gal and AFU without overlapping detection of both enzymes. This dual-channel probe exclusively differentiated between normal and senescent cells based on the high expression of b-gal or AFU, as demonstrated by human hepatoma cells (HepG2 cells), Ovcar-3 cells, and mouse breast 4T1 tumour cells. Moreover, the probe can be used as an effective alternative for tracing b-gal and AFU during tumour senescence in mice, making it a promising tool in biomedical research and clinical medicine.[110] Another recent study by Williams *et al.* shows that they used a two-colour diffuse *in vivo* flow cytometry (DiFC) system to detect circulating cells that express two distinct fluorescent proteins of the tumor. They found that GFP or tdTomato as two-colour DiFC can detect two populations of circulating tumor cells (CTCs) and CTC clusters (CTCCs) concurrently. Additionally, this instrument could allow study of tumor development and response to therapies for different sub-populations in the same animal.[111] Furthermore, Hama and colleagues developed a novel activatable fluorophore to improve MI in peritoneal ovarian metastases and discovered that self-quenching avidin-rhodamine X (Av-ROX), which binds to lectin on cancer cells, is triggered after endocytosis and destruction in the lysosomes. Using this strategy in a mouse model of peritoneal ovarian metastases provides a generalizable and extremely sensitive means of detecting cancer microfoci *in vivo* for surgical and endoscopic treatments. Hence, they confirmed that the sensitivity and specificity of Av-3ROX for detecting ovarian cancer are less than 0.8 mm and 98%, respectively.[112] Moreover, the surface of silica nanoparticles can be altered in several ways by linking various functional groups and could be utilized as a fluorescent agent. For instance, based on the Wang *et al.* study, silica particles exhibit enhanced fluorescence when they are bonded to aggregation-induced emission (AIE) dyes *via* non-covalent interactions. Together with the AIE dyes, aptamer-linked functionalized particles have a high degree of selectivity in targeting MCF 7 cells, and fluorescence is produced when NPs aggregate in that area. This strategy can eliminate confusion and false positive results.[113] Another investigation showed that QDs CdTe/CdS/ZnS highly functionalized with mPEG (methoxy PEG) demonstrated a significant reduction in ZnS deposition, an improvement in colloidal stability appropriate for curing solid tumors, and an enhanced binding affinity with a little 3% drop in fluorescence. Therefore, through confocal imaging, cellular connections were readily visible as a result of increased binding affinity.[114] It is reported that porphyrin not only can be employed in photodynamic therapy as a photosensitizer but also could be used as a fluorescent agent in FI. However, Secret *et al.* demonstrated that NPs coupled to photosensitizers such as porphyrin *via* covalent bonds can also perform Two Photon Excitation (TPE) by transferring energy to the porphyrin after stimulating the silica particle. Consequently, TPE enables deeper imaging, and silica particles containing mannose moieties aid in locating the targeted cells.[115] Zwitterion ligands attached to quantum dots are another nanostructure that has been used by Tasso and colleagues in cellular imaging. They found out that in both live and fixed cells, these QD nanobioconjugates exhibit a high selectivity for internal and extracellular targets. Therefore, the dithiol/zwitterion QD-protein A nanoconjugates have the latent potential to develop into a commercially available tool that will help answer unanswered biological issues.[116] Studies by Ag *et al.* developed a water-soluble thioglycolic acid TGA-capped CdTe/CdS quantum dots (TGA-QDs) conjugated to anti-human epidermal growth factor receptor 2 (HER2) antibodies to target HER2-overexpressing cancer cells. Ag and colleagues reported that antibody-conjugated to TGA-QDs showed increased fluorescence signals in cells overexpressing HER2 compared cells not expressing this receptor, showing great potential for targeted cellular imaging studies (see Fig. 4 and 5).[117] Liang *et al.*

Table 3 Some in vitro, in vivo and clinical studies are summarized[a]

Fluorescence material or complex	Type of study (in vitro, in vivo and clinical)	Type of tumor or cell line	References
Green FP (GFP) or tdTomato	In vitro and in vivo	MM.1S cells and 4T1 cells	111
Avidin-rhodamine X (Av-ROX)	In vitro and in vivo	Peritoneal ovarian metastases (SHIN3)	112
Aptamer and AIE linked slica NPs (Apt-AIE slica NPs)	In vitro and in vivo	MCF 7 cells	113
Methoxy PEG attached to quantum dots	In vitro	A549 cell lines	114
Porphyrin	In vitro	MCF-7 human breast cancer cells	115
Zwitter ion ligands attached to quantum dots	In vitro and in vivo	HeLa cells	116
N-CDots	In vitro	3T3 and HepG2 cells	118
Multiple layers of tryphtophan is attached to AuNPs	In vitro	Escherichia coli cells	119
NOTA	In vitro and in vivo	Prostate and breast	120 and 121
CRANAD-164	In vitro and in vivo	Liver and serum samples	122
P-Cy	In vitro and in vivo	A549	123
Probe ZHJ-X	In vitro	MCF-7 cells, HL60 cells and zebrafish	124
ALA-PpIX and ICG	In vivo	Glioma	125
ICG	Clinical	Penile cancer lymph	126
Alexa Fluor 647 and Cy3B	In vitro and in vivo	LNCaP cell line	127
[64]Cu-BMV101/ABP BMV109	In vitro and in vivo	Macrophages cells and cardiovascular system	128
Cetuximab-800CW	Clinical trial	Oral cancer	129
EGFR-FITC-SiO$_2$-NPs	in vitro and in vivo	Head and neck	130
MHI-148	in vitro and in vivo	Lung cancer	46
B7-H3-ICG agent	in vitro and in vivo	Breast cancer	131
Cell immunoglobulin domain and mucin domain 3 – IRDye-800CW (TIM3-800CW)	In vivo	Glioblastoma	132
CRANAD-102-AβOs	In vitro and in vivo	Alzheimers disease (AD)	

[a] AIE, aggregation-induced emission; N-Cdots, N-doped carbon dots; ALA-PpIX 5-aminolevulinic acid-protoporphyrin (IX); MHI-148, near-infrared heptamethine cyanine dye; EGFR, human epidermal growth factor receptor; SiO$_2$, silica; ICG, indocyanine green; B7-H3, B7 homolog 3 protein.

reported that nitrogen-rich carbon dots (N-CDots), besides demonstrating low toxicity in 3T3 and HepG2 cells, also could be used for imaging living cells because of their brilliant FI in blue to red. These findings showed that N-CDots, one type of precise probe, can be employed in a number of contexts, including environments and in vitro imaging.[118] Multiple layers
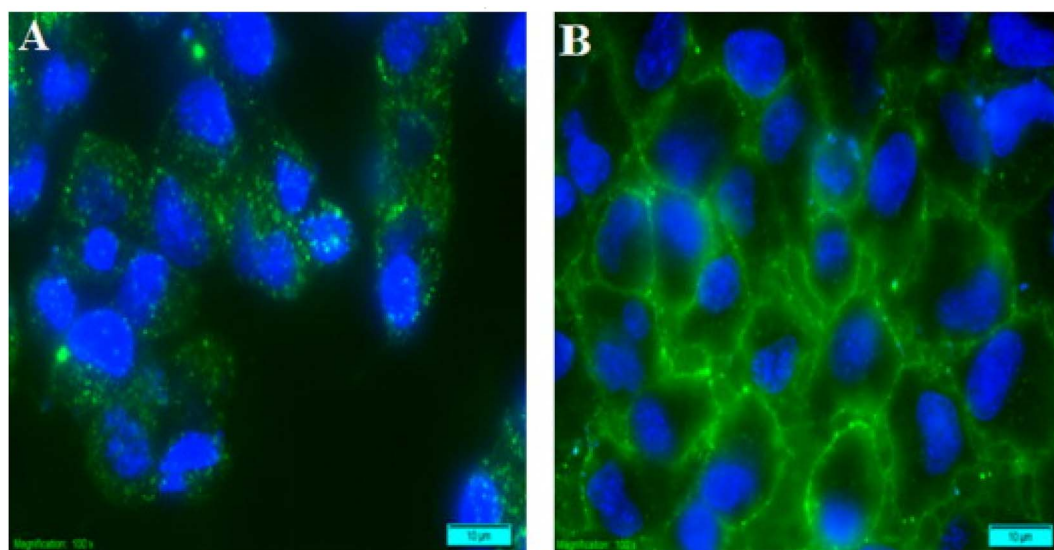

Fig. 4 Fluorescence microscopy imaging of A549 cells. Cells were treated with TGA–QDs (green) for 2 h at 37 °C, (A) overlap of two images, control nuclei staining with DAPI (blue). Cells were treated with TGA–QDs for 2 h at 4 °C, (B) overlap of two images, control nuclei staining with DAPI. Anti–HER2 TGA–QDs showed a high binding affinity for A549 cells, which resulted in strong fluorescent signals. Reproduced from ref. 117 with permission from Elsevier, copyright 2014.
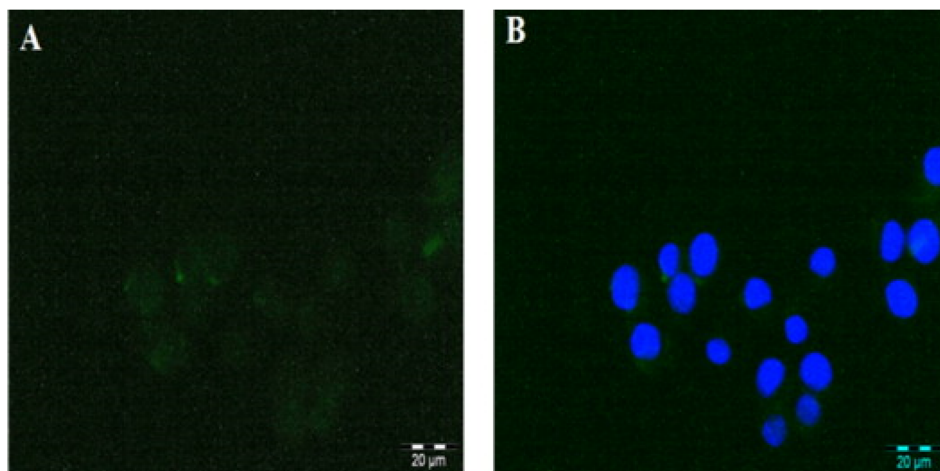
Fig. 5 Fluorescence microscopy images of NIH-3T3. (A) Cells were treated with TGA-QDs/anti-HER2 for 2 h at 37 °C, (B) overlap of two images, control nuclei staining with DAPI. Anti-HER2 TGA-QDs showed poor binding affinity for NIH-3T3 cells, as demonstrated by low fluorescence signals compared to those in A549 cells. Reproduced from ref. 117 with permission from Elsevier, copyright 2014.

of tryptophan attached to AuNPs have been synthesised by Pajovic *et al.*, which showed that functionalizing AuNPs with several layers of tryptophan showed different fluorescence characteristics in deep ultraviolet imaging due to tryptophan's UV absorption and emission. However, the coupling of tryptophan amino acid with gold nanoparticles produced biocompatible hybrid entities with the ability to absorb and emit light.[119] Furthermore, in several studies dual PET and near-infrared FI probes have been used as tools for imaging in oncology. For instance, copper-64 (^{64}Cu) is traditionally the most popular isotope for systemic monoclonal antibodies (mAb) imaging. A trastuzumab and an EpCAM application are notable for imaging metastases of some cancers, such as prostate and breast. The targeting of CD133-expressing U251 glioblastomas by use of separately labelled PET (^{64}Cu-triazacyclononanetriacetic acid (NOTA)) and fluorescent (Alexa Fluor 680, BODIPY) AC133 mAbs allows imaging in the brain tumors.[120,121] A recent study by Yang *et al.* designed a series of half-curcumin-based chemiluminescence probes (CRANAD-123, CRANAD-162, CRANAD-163 and CRANAD-164) for FI *in vitro* and *in vivo*. Their findings showed that CRANAD-164 could be used to detect quasi-stable oxidised proteins (QSOP) *in vivo* and in patient serum samples. Finally, they suggested that CRANAD-164 can be used to monitor the increase of QSOP during ageing.[122] Another new fluorescent probe was designed and synthesized by Duan *et al.* called P-Cy *via* photo-induced electron transfer technique to image the cysteine (Cy) level *in vivo*. They found that P-Cy has low cytotoxicity, great selectivity, and good sensitivity for FI of cysteine level in A549 cells *in vitro* and *in vivo*.[123] In a similar study, Zhou and co-workers used ZHJ-X based on cyanobiphenyl (a new fluorescent group) to detect cysteine in live cells such as MCF-7 cells, HL60 cells and zebrafish. Their results illustrated that probe ZHJ-X has a faster and more effective detection capability and can be utilised for precise Cys recognition.[124] Scorzo *et al.* used fluorescence cryotomography to evaluate and compare the 3D spatial distributions of 5-aminolevulinic acid-protoporphyrin (IX) (ALA-PpIX)

and second-window ICG in a pig brain that has gliomas. They revealed that there are notable distinctions in spatial distributions between the two agents significantly. While ALAPpIX was more visible in the tumor edge, ICG accumulated inside the tumor core. Both second-window ICG and ALA-PpIX demonstrated increased contrast between the tumor and the backdrop.[125] A clinical study by Hora *et al.* shows that ICG has been applied in men to identify the sentinel lymph node with penile cancer, and they noted during video endoscopic inguinal lymph node dissection (VEILND), the sentinel lymph node is more visible when using a fluorescence infrared picture with ICG dye. Even though the ICG dose of 2.5 (5) mg diluted in 1 ml can be administered preoperatively in the superficial area, 16.7% of them have an inexplicable failure of ICG marking.[126] Kwon *et al.* synthesised a dual probe from Alexa Fluor 647 and Cy3B for FI of prostate cancer (prostate-specific membrane antigen or PSMA) margin assessment. This dual probe caused a significant contrast difference between the PSMA-positive tumors and their surrounding normal tissues (muscle, adipose, and prostate), which was revealed by the ratiometric dual probe difference specimen imaging (DDSI) technique.[127] In another study, dual-modality activity-based probes (^{64}Cu-BMV101 and ABP BMV109) were used as MI agents for vascular inflammation. Mouse models of atherosclerosis showed that activity-based probes (ABPs) that target cysteine cathepsins can be utilised to noninvasively image active macrophage populations using both optical and PET/CT techniques. Similar particular labelling of active macrophage populations can be seen when the probes are applied topically to human carotid plaques. Moreover, fluorescence molecular tomography (FMT) was used to noninvasively examine the mice two weeks following surgery at an excitation/emission wavelength of 680/700 nm.[128] EGFR-targeted FMI for assessment of cancer has been reported in a few clinical trials. For example, Wit *et al.* employed cetuximab-800CW in oral cancer for intraoperative margin assessment in 65 patients with 66 tumors. Data showed fluorescent spots identified in the surgical margin with 100% sensitivity, 85.9%
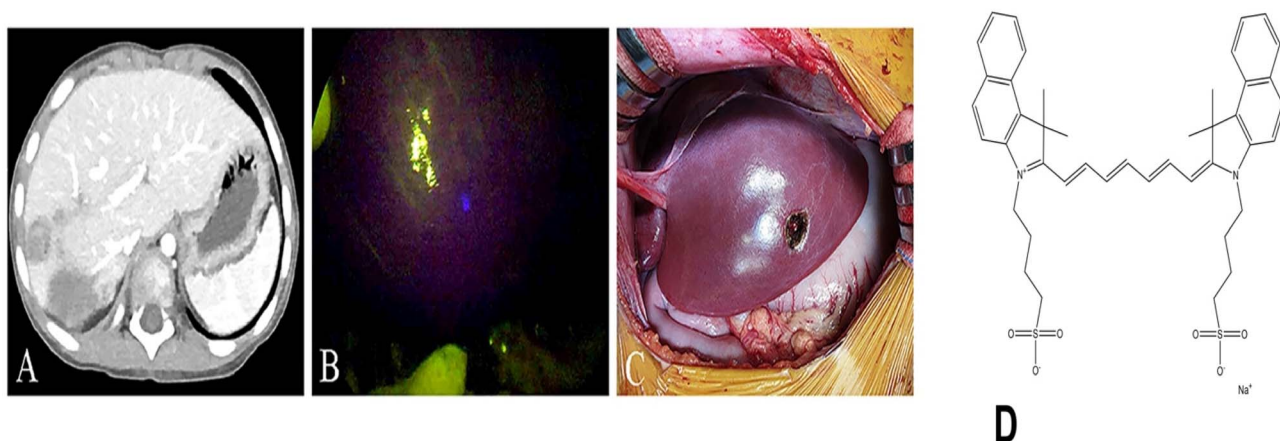
Fig. 6 Intraoperative ICG fluorescence imaging of a hepatoblastoma nodule not visualised on preoperative CT scan. (A) Preoperative CT scan showing no sign of the nodule (B) the same nodule clearly visualized under ICG/NIR fluorescence during surgery (C) gross pathological specimen of the resected nodule, confirming hepatoblastoma adapted from [135] under the terms of the Creative Commons CC BY 4.0 license (D) chemical structure of ICG.

specificity, 58.3% positive predictive value and 100% negative predictive value.[129] Another study revealed that silica NPs modified with the fluorescence stain fluorescein isocyanate (FITC) can be used for particle detection and with EGFR targeting antibodies (EGFR-FITC-SiO$_2$-NPs) for enhanced tumor specificity.[130] It is reported that MHI-148 dye can penetrate the cytoplasmic membrane of lung cancer cells and stain tumor cells 1 h after injection *in vivo*.[46] Wilson *et al.* used anti-B7-H3-antibody-ICG as a dual contrast agent in breast cancer. They concluded that the B7-H3-ICG agent can assess the disease status of tissues with high diagnostic accuracy, intraoperatively with high resolution, sensitivity and specificity.[131] Zhang *et al.* used the TIM3-800CW probe for FI to detect checkpoint inhibitor protein in glioblastoma in C57BL/6 mice. They observed that TIM3-800CW can emit a signal at 800 nm from the checkpoint inhibitor protein (TIM3 expression).[132] The most recent study by Liu *et al.* shows that FI can be useful to diagnose Alzheimer's disease (AD). They used the CRANAD-102-AβOs02-AβOsobe to target amyloid-β oligomers (AβOs) protein, crucial toxic proteins in early AD, and *in vitro* and *in vivo* imaging depicted that the CRANAD-102-AβOs probe has a high affinity for AβOs, emission in the near-infrared region, good biocompatibility and a valuable NIRF probe for early detection of AD and a useful tool to follow up AD pathological mechanisms.[133]

A study performed by Feng and colleagues investigated the safety and practicality of indocyanine green (ICG) fluorescence imaging during paediatric cancer surgeries. Their study involved 7 patients (which entailed 4 cases of Wilms tumours, 1 malignant rhabdoid tumour and 2 renal cell carcinomas); they noted that administering IGG intravenously (at doses ranging from 2.5 to 5 mg) allowed tumour visualisation in 6 out of 7 cases. The tumours showed different fluorescence patterns: Wilms tumours and renal cell carcinomas were hypofluorescent, while the malignant rhabdoid tumours were hyperfluorescent. ICG was also found to be effective in 3 patients. Importantly, it did not cause any unwanted complications.

However, some limitations were noted, such as compromised visualisation when tumours were adhered to surrounding tissues or after preoperative renal artery embolisation. Feng and colleagues concluded that ICG guidance can enhance nephron-sparing surgery and lymph node resections in children, but it remains imperative to optimise the dosing and surgical techniques.[134]

Another study conducted by Cho *et al.* demonstrated that intraoperative ICG fluorescence imaging (0.3 mg kg^{-1} IV, 24–48 hours prior to surgery) substantially improved the intraoperative identification and excision of paediatric hepatoblastoma. ICG identified tumours that were missed by CT scans before surgery on 22 occasions in 17 patients (Fig. 6), achieved a median safety margin of 6 mm, and allowed resection of lung metastases and vascular reconstruction in liver transplants. Major drawbacks were false positives in 8/22 lesions (*e.g.*, benign nodules less than 10 mm) and inability to visualise tumours larger than 10 mm deep.[135]

6. Comparison sensitivity and specificity of FI with other modalities

FI, PET and SPECT are important techniques in molecular imaging, each with its own advantages and limitations in terms of image resolution, sensitivity and specificity. FI has been under extensive investigation due to its high sensitivity, specificity (ability to selectively label molecules and structures of interest) and simplicity, as well as its high spatial resolution, which facilitates the intricate visualisation of cellular and subcellular structures. Furthermore, FI allows for real-time monitoring abilities whereby biological processes such as cellular differentiation, migration and interaction with surrounding tissue can be captured at the moment.[136,137]

FI has shown high sensitivity, particularly in detecting superficial lesions depending on the application and dye used.[138–140] Therefore, it is only applicable for superficial

Table 4 FI has been compared with PET and SPECT in MI

Aspect	FI	PET imaging	SPECT	Reference
Sensitivity	High, especially for small-scale or surface targets	Very high, especially for deep tissue and low concentrations	Moderate to high, sensitive to large-scale processes	151–156
Specificity	High, with selective probes but prone to background noise	Moderate to high, depending on the radiotracer. Off-target binding possible	High, with appropriate radiotracers	143, 144, 149 and 157
Resolution	High spatial resolution, limited by tissue depth	Lower spatial resolution compared to fluorescent imaging	Lower (millimeter scale)	158–162
Depth of penetration	Superficial target (limited by tissue scattering and absorption)	Excellent depth penetration, suitable for full-body imaging	Deep (penetrates through tissues)	163, 164 and 165
Quantification	Quantification of FI is very difficult due to noise	Can provide quantitative functional data	Can provide quantitative functional data	150 and 166–169
Clinical use	Primarily in preclinical research	Widely used in clinical settings (oncology, cardiology, neurology)	Clinical (functional imaging, diagnostics)	149,170 and 171
Limitations	Limited tissue penetration, autofluorescence	Lower spatial resolution, radiation exposure and expensive	Lower spatial resolution, radiation exposure	170,172 and 173

imaging (up to 1 cm),[141,142] which has propelled the investigation of probes that have a superior tissue penetration depth. Emile and colleagues investigated the overall sensitivity and specificity of indocyanine green (ICG) near-infrared (NIR) fluorescence in sentinel lymph node (SLN) detection in colorectal cancer (CRC). The studies noted that the median sensitivity, specificity, and accuracy rates were 73.7, 100, and 75.7. The pooled sensitivity and specificity rates were 71% and 84.6%. This suggests that ICG-NIR fluorescence is a promising technique for detecting SLNs in CRC.[143]

PET is a nuclear medicine imaging technique that uses radioactive tracers for early detection and treatment follow-up of many diseases, including cancer.[144] PET is highly sensitive and is capable of detecting extremely low concentrations of tracers (femtomolar range). However, its specificity hinges on the type of tracer used. This technique allows for whole quantitative imaging, making it an indispensable tool in oncology, cardiology and neurology. Risks associated with contrast administration, such as potential anaphylaxis and contrast-induced nephropathy, accompany PET. However, the radiotracers used generally have insignificant side effects.[144–146] SPECT is another widely used nuclear imaging technique that provides three-dimensional information about the functional and molecular processes within the patient's body and is less expensive and more readily available compared to PET.[147,148] Its sensitivity and specificity main depend on the application. For example, SPECT has shown an 82% sensitivity and a 76% specificity in myocardial perfusion testing for the diagnosis of coronary artery disease. Furthermore, the annual risk of adverse cardiac events is less than 1% for patients with normal myocardial SPECT imaging. When it comes to brain imaging for Alzheimer's disease diagnosis, SPECT has a 92% sensitivity, 100% specificity, 92% positive predictive value, and 57% negative predictive value.[149] However, SPECT generally exhibits lower spatial resolution compared to FI and PET. Moreover, attenuation and scatter corrections continue to pose significant challenges in achieving precise quantitative outcomes with SPECT.[150] Here in Table 4, based on the reviewed data, a brief comparison of FI with PET and SPECT has been performed.

7. Novel technologies and interdisciplinary applications in FI

To improve sensitivity, specificity, resolution, penetration depth and clinical practicality, researchers are diving into new tools that could really enhance the overall efficiency of FMI.[174,175] Recent advancements have led to the development of smart nanoprobes, carbon dots (CDs) in particular. They have gained a lot of attention lately due to their remarkable versatility and impressive optical properties, such as adjustable emission wavelengths, high quantum yield and excellent photostability. CDs are ideal for various applications including biomedical imaging due to many advantages ranging from biocompatibility, low toxicity and ease of surface modification.[176,177] Furthermore, their tunable optical properties and exceptional sensitivity allow them to serve as fluorescent probes for detecting pH, heavy metal ions and other analytes.[176,178] Various studies have used green fluorescence CDs and a related probe with fluorescence activation to visualise and detect cancer.[179,180] CDs were coated with folic acid to selectively capture images of cancers. With turn-on fluorescence, the probe distinguishes cells that were positive for the folate receptor (FR). In another study, folic acid-conjugated fluorescent CDs were synthesised to exclusively bind to FR. With FR, these CDs were able to differentiate between healthy cells and A549 adenocarcinoma human basal epithelial cancer cells and displayed notable biocompatibility.[181] Two-dimensional (2-D) materials such as graphene

oxide or transition metal dichalcogenides are used to alter fluorescent quenching and recovery in biosensing, which is attributed to their unique electronic properties. Organic fluorophores, such as BODIPY, are functionalised with these materials to enhance sensitivity and photostability.[182–185]

In recent years, DNA origami-enabled optical biosensors have gained popularity in biological applications, particularly in sensing and imaging. This technology can offer a predictable, programmable and addressable nanoscale scaffold for the precise assembly of various kinds of molecules, such as fluorophores and targeting moieties, to actively identify and quantify biomarkers and microenvironmental alterations at the single-molecule level. DNA origami biosensors offer an impressive single-molecule resolution and a high signal-to-noise ratio, underscoring them as excellent alternatives to conventional analytical methods.[186–188] There has been significant progress in circumventing limitation posed by traditional fluorescence, primarily poor penetration depth and scattering. TTA-UC is highly promising as far as this is concerned since photon upconversion leverages high-energy excited states from low-energy photons.[189,190] Such photons, particularly in the red and near-infrared wavelength ranges, can penetrate tissue more deeply and experience less competitive absorption in coloured reaction media, thereby enhancing the efficiency of large-scale reactions and *in vivo* phototherapy.[190] TTA-UC, in particular, demonstrates high upconversion efficiencies, requiring low excitation power densities and featuring tunable absorption and emission wavelengths. Consequently, this facilitates high-resolution imaging in deep-seated tissues without the need for high-power pulsed lasers, thus minimising unwanted phototoxic effects.[190–192] In addition to this, time-gated (TGI) techniques effectively attenuate short-lived autofluorescence and scattered light by exclusively detecting the long-lived emission of specific lanthanide-based probes or phosphorescent molecules.[193,194] This not only optimises the signal-to-background ratio (SBR) at depth but also allows for visualization of targets embedded within convectional continuous wave imaging. The combination of these techniques could transform non-invasive deep-tissue FMI.[193,195–198] Artificial intelligence (AI) has shown significant promise in biomedical research, particularly in imaging. The incorporation of AI, such as machine learning algorithms helps to enhance fluorescence imaging and is poised to improve image quality by reducing noise in low-light FMI data, maintaining the biological information.[199–201] Furthermore, super-resolution imaging has the capability to resolve objects below the classical diffraction limit of optical resolution.[202] Its integration of AI not only improves image quality but also opens up new avenues for innovative imaging techniques for advanced microscopy. This technique uses AI algorithms, such as deep learning models like Convolutional Neural Networks (CNNs) and Generative Adversarial Networks (GANs), able to reconstruct and enhance image resolution in fluorescence microscopy.[203–206] FMI is widely used in a variety of scientific disciplines due to its versatility. FMI probes allow for real-time imaging of neurotransmitter action with exceptional resolution in neuroscience, as demonstrated by genetically encoded dopamine sensors combined with enhanced GFP variants, which allow for the imaging of chemical signalling in live neural circuits.[207–209]

With immunotherapy, the combination of organic small-molecule fluorescent probes with immune system-related molecules (enzymes/small-molecules), it is possible to visualize the activation status of relevant immune cells during abnormal immune processes, thus allowing timely adjustments to the immunotherapy regimen and improving the efficacy of immunotherapy.[210] Despite significant progress in preoperative workup and surgical planning, surgeons often rely on their eyes during surgical excision procedures. This can be arduous in some patients, which calls for intraoperative guidance. NIR fluorescence has been highly recommended to guide surgeons during surgery. Therefore, fluorescent-guided surgery can allow for real-time imaging during an operation.[211,212] For instance, ICG is a widely used fluorophore owing to its good safety profile, which has led to utility in executing dedicated intraoperative imaging systems that allow blood flow measurements during cardiac and transplantation surgery.[213] Lastly, FI probes such as quantum dots can be used in other fields such as agriculture and environmental science, whereby they are conjugated to targeting moieties to actively identify and detect pollutants and certain microbes affecting crops.[214,215]

8. Conclusion and prospective view

This review examines recent advances in fluorescent materials for FMI, focusing primarily on innovative approaches in probe modelling, clinical utility, and imaging technologies. We highlighted significant progress in the development of cutting-edge materials, such as BODIPY derivatives, to facilitate active-targeted cancer imaging, NIR dyes (*e.g.*, MHI-148) endowed with tumour specificity, and TTA-UC nanoparticles for reaching deep-seated tissues. Collectively, these innovations address major limitations of traditional fluorescent materials, specifically relating to poor photostability, sensitivity, and biocompatibility. We further examined significant efforts made to enhance outcomes in clinical and preclinical studies, which involved the application of ICG-guided sentinel lymph node mapping and activatable probes like Av-ROX to track metastasis, as well as combinatorial strategies of PET/NIR agents for oncology. Furthermore, we mentioned new technologies such as DNA origami biosensors, AI-driven imaging analysis, and time-gated imaging, which will revolutionise imaging, in terms of resolution, quantification, and noise reduction. In this review, the comparison of FMI *versus* modalities like PET and SPECT warrants the need to optimise multimodal integration and clinical translation.

Fluorescence materials and fluorescence imaging have become pivotal in molecular imaging, offering high-resolution, real-time and non-invasive insights into biological processes. Key advantages of fluorescence imaging include its sensitivity, versatility and the ability to track dynamic processes in living organisms with minimal tissue disruption. The development of advanced fluorescent materials such as quantum dots, organic fluorophores, and fluorogenic probes has been significantly improved and led to promoting the specificity and sensitivity of

fluorescence imaging as a powerful tool for diagnosing and monitoring diseases.

So far, the findings show that the last challenges of FI can be categorized into technical, biological and material-related concerns. For instance, signal-to-noise ratio (SNR) is crucial for obtaining high-quality images, but the fluorescence signal can be weak, especially when imaging deep tissues. This often results in low-resolution or noisy images. Another limitation is photobleaching, where the fluorophores lose their ability to emit light after prolonged exposure to excitation light, which is a major issue in long-term imaging. Moreover, repeated cycles of fluorescence exposure can also degrade fluorophores, limiting the duration of imaging experiments. Fluorescence signals are often weakly detected from deep tissues due to scattering and absorption of light by the tissue. Consequently, this limits the imaging to superficial regions or requires the use of advanced techniques (like multiphoton microscopy), which may have limitations in terms of resolution or complexity. Many tissues and biological structures exhibit autofluorescence when exposed to UV light, which overlaps with the fluorescence of the target fluorophores. This contamination can make it difficult to distinguish the signal from the background, especially in tissues like the brain or liver. Deep-tissue imaging requires highly sensitive detectors and improved optical methods. Achieving high-resolution 3D imaging at greater depths is challenging, especially with conventional fluorescence microscopy, which is typically limited to imaging at surface or sub-surface levels. Despite the progress in fluorescent probe development, there is still a lack of ideal fluorescence materials for many specific imaging needs. Fluorophores with desirable properties, like high brightness, long emission wavelengths (for deep tissue penetration), high photostability, and minimal toxicity, are often hard to design and produce, limiting their practical use in molecular imaging. Developing fluorescent probes that can specifically target desired molecules or cells (such as cancer cells or specific receptors) without affecting surrounding tissues is a major challenge. Non-specific binding or the inability to precisely target biomarkers can lead to false signals or misinterpretation of data. Many fluorescent materials, particularly those based on heavy metals (like quantum dots), have concerns regarding their toxicity or potential long-term effects on living systems. There is a constant need for the development of biocompatible fluorophores that can be safely used *in vivo* over extended periods. FMI often lacks quantitative accuracy due to variations in tissue scattering, fluorophore distribution and background noise. Achieving reliable, reproducible measurements of fluorophore concentration in tissues remains difficult. Real-time, longitudinal monitoring of disease progression or therapeutic response using fluorescence imaging is limited by the above challenges, including depth resolution, tissue penetration, and fluorophore stability. For example, it can be difficult to track the exact distribution of a fluorescent probe over time *in vivo* without significant interference from the body's own fluorescence or scattering.

In the future, more emphasis should be placed on developing highly reproducible functionalization procedures and incorporating diverse nanoprobes to improve molecular imaging, which can provide validated clinical applicability. The functionalization of many molecules should be attempted in a single process using a common ligand/attaching chemical compound. Furthermore, the integration of nanotechnology with fluorescence materials promises more efficient, targeted and biocompatible imaging agents. Nanoparticles like quantum dots and metal nanoclusters are expected to become more widely used due to their tunable optical properties and potential for multimodal imaging. Additionally, the development of activatable fluorescent probes, which become fluorescent only in the presence of specific biological conditions, will enhance the selectivity and reduce background interference. Moreover, while fluorescence imaging has traditionally been limited by tissue depth due to scattering and absorption, innovations such as enhanced fluorescent probes and improved optical techniques (*e.g.*, tissue clearing and multi-photon microscopy) are expected to extend its capabilities to deeper tissues, facilitating non-invasive imaging of whole organisms and complex anatomical regions. When dealing with lighting issues, employing a visible light source that does not contain 840 nm or longer wavelengths can be the ideal answer. One approach is to use a short-wavelength pass filter, which removes long wavelengths from a typical headlight system. Surgical lighting systems are increasingly switching from halogen lights to light-emitting diodes (LEDs) due to their longer life, lower energy usage, and lower heat emission. LEDs produce light with a very limited range of wavelengths; thus, it is theoretically possible to create a surgical illumination system utilising LEDs that does not interfere with fluorescence imaging. Finally, combining fluorescence imaging with other modalities (*e.g.*, MRI, PET, CT) to provide comprehensive information is still challenging. Multimodal imaging techniques require advanced hardware and software that can accurately integrate the data from multiple imaging systems, and issues such as registration accuracy and data fusion still need to be improved. Moreover, the combination of artificial intelligence (AI) with fluorescence imaging will revolutionize data analysis, providing more accurate interpretations of imaging results. Automated image segmentation, quantification and pattern recognition will accelerate the process of diagnostics, offering personalized treatment strategies.

Data availability

No data was used for the research described in the article.

Author contributions

Conceptualization and acquisition of data, N. W. N and K. M.; writing—original draft preparation, N. W. N and K. M. Writing—review and editing, B. P. G. and H. A.; supervision, B. P. G. and H. A. All authors have read and agreed to the published version of the manuscript.

Conflicts of interest

The authors do not have conflicts of interest to disclose.

Acknowledgements

References

1 R. A. Sheth, P. Heidari, S. A. Esfahani, B. J. Wood and U. Mahmood, *Radiology*, 2014, **271**, 770–777.

2 H. Li, Q. Gong and K. Luo, *Theranostics*, 2024, **14**, 4127–4146.

3 D.-E. Oprea-Lager, S. MacLennan, A. Bjartell, A. Briganti, I. A. Burger, I. de Jong, M. De Santis, U. Eberlein, L. Emmett, K. Fizazi, S. Gillessen, K. Herrmann, S. Heskamp, A. Iagaru, B. A. Jereczek-Fossa, J. Kunikowska, M. Lam, C. Nanni, J. M. O'Sullivan, V. Panebianco, E. Sala, M. Sathekge, R. Sosnowski, D. Tilki, B. Tombal, G. Treglia, N. Tunariu, J. Walz, D. Yakar, R. Dierckx, O. Sartor and S. Fanti, *Eur. Urol.*, 2024, **85**, 49–60.

4 K. E. Guja, G. Behr, A. Bedmutha, M. Kuhn, H. R. Nadel and N. Pandit-Taskar, *Semin. Nucl. Med.*, 2024, **54**, 438–455.

5 O. Shimomura, F. H. Johnson and Y. Saiga, *J. Cell. Comp. Physiol.*, 1962, **59**, 223–239.

6 R. Y. Tsien, *Annu. Rev. Biochem.*, 1998, **67**, 509–544.

7 R. B. Sekar and A. Periasamy, *J. Cell Biol.*, 2003, **160**, 629–633.

8 E. L. Schmidt, Z. Ou, E. Ximendes, H. Cui, C. H. C. Keck, D. Jaque and G. Hong, *Nat. Rev. Methods Primers*, 2024, **4**, 1–22.

9 na Li, M. Wang, J. Zhou, Z. Wang, L. Cao, J. Ye and G. Sun, *Eur. J. Med. Chem.*, 2024, **267**, 116173.

10 X. Wang, Y. Liu, X. Wang, X. Ye, W. Cheng, G. Chen, H.-L. Zhu, J. Zhao and Y. Qian, *Biosens. Bioelectron.*, 2023, **238**, 115563.

11 L. Hao, F. Liu, X. Wang, L. Kang, Y. Wang, L. Wang, Z. Lin and W. Zhu, *Small*, 2024, **20**, 2308470.

12 J. A. Stibbe, P. Hoogland, F. B. Achterberg, D. R. Holman, R. S. Sojwal, J. Burggraaf, A. L. Vahrmeijer, W. B. Nagengast and S. Rogalla, *Mol. Imaging Biol.*, 2023, **25**, 18–35.

13 H. Luo and S. Gao, *J. Controlled Release*, 2023, **362**, 425–445.

14 V. Ntziachristos, *Annu. Rev. Biomed. Eng.*, 2006, **8**, 1–33.

15 S. Knutson, E. Raja, R. Bomgarden, M. Nlend, A. Chen, R. Kalyanasundaram and S. Desai, *PLoS One*, 2016, **11**, e0157762.

16 M. L. James and S. S. Gambhir, *Physiol. Rev.*, 2012, **92**, 897–965.

17 S. Achilefu, *Chem. Rev.*, 2010, **110**, 2575–2578.

18 S. S. Kelkar and T. M. Reineke, *Bioconjugate Chem.*, 2011, **22**, 1879–1903.

19 Y. Zhang, S. Li, H. Zhang and H. Xu, *Bioconjugate Chem.*, 2021, **32**, 4–24.

20 A. Alibakhshi, F. Abarghooi Kahaki, S. Ahangarzadeh, H. Yaghoobi, F. Yarian, R. Arezumand, J. Ranjbari, A. Mokhtarzadeh and M. de la Guardia, *J. Controlled Release*, 2017, **268**, 323–334.

21 M. A. Mir, U. Mehraj, B. A. Sheikh and S. S. Hamdani, *Hum. Antibodies*, 2020, **28**, 29–51.

22 I. Vaneycken, N. Devoogdt, N. Van Gassen, C. Vincke, C. Xavier, U. Wernery, S. Muyldermans, T. Lahoutte and V. Caveliers, *Faseb. J.*, 2011, **25**, 2433–2446.

23 J. Boonyaratanakornkit and J. J. Taylor, *Front. Immunol.*, 2019, **10**, 1694.

24 S. Wang, Y. Li, J. Mei, S. Wu, G. Ying and Y. Yi, *Int. J. Biol. Macromol.*, 2024, **275**, 133730.

25 J. A. Kiernan, *Color. Technol.*, 2006, **122**, 1–21.

26 J. Weber, P. C. Beard and S. E. Bohndiek, *Nat. Methods*, 2016, **13**, 639–650.

27 S. B. van der Meer, T. Knuschke, A. Frede, N. Schulze, A. M. Westendorf and M. Epple, *Acta Biomater.*, 2017, **57**, 414–425.

28 L.-Y. Wei, K.-S. Huang, H.-H. Lin, Y.-P. Wu, K.-T. Tan, Y. Y. Lee and I.-C. Chen, *J. Phys. Chem. C*, 2018, **122**, 28431–28438.

29 M. Koch, P. Symvoulidis and V. Ntziachristos, *Nat. Photonics*, 2018, **12**, 505–515.

30 T. Kim, C. O'Brien, H. S. Choi and M. Y. Jeong, *Appl. Spectrosc. Rev.*, 2018, **53**(2–4), 349–359.

31 M. Tian, *J. Nucl. Med.*, 2015, **56**, 329.

32 K. M. Dean and A. E. Palmer, *Nat. Chem. Biol.*, 2014, **10**, 512–523.

33 J. Mao and H. He, *J. Intell. Med.*, 2024, **1**, 42–62.

34 P. P. P. Kumar, S. Saxena and R. Joshi, *Colorants*, 2025, **4**, 13.

35 S. Wang, L. Gai, Y. Chen, X. Ji, H. Lu and Z. Guo, *Chem. Soc. Rev.*, 2024, **53**(8), 3976–4019.

36 M. Lledos, D. G. Calatayud, F. Cortezon-Tamarit, H. Ge, C. Pourzand, S. W. Botchway, M. Sodupe, A. Lledós, I. M. Eggleston and S. I. Pascu, *Chem.–Eur. J.*, 2024, **30**, e202400858.

37 J. Pliquett, A. Dubois, C. Racoeur, N. Mabrouk, S. Amor, R. Lescure, A. Bettaïeb, B. Collin, C. Bernhard, F. Denat, P. S. Bellaye, C. Paul, E. Bodio and C. Goze, *Bioconjugate Chem.*, 2019, **30**, 1061–1066.

38 F. de Jong, J. Pokorny, B. Manshian, B. Daelemans, J. Vandaele, J. B. Startek, S. Soenen, M. Van der Auweraer, W. Dehaen, S. Rocha and G. Silveira-Dorta, *Dyes Pigm.*, 2020, **176**, 108200.

39 Y. Ni, L. Zeng, N.-Y. Kang, K.-W. Huang, L. Wang, Z. Zeng, Y.-T. Chang and J. Wu, *Chem.–Eur. J.*, 2014, **20**, 2301–2310.

40 D. Jurgutis, G. Jarockyte, V. Poderys, J. Dodonova-Vaitkuniene, S. Tumkevicius, A. Vysniauskas, R. Rotomskis and V. Karabanovas, *Int. J. Mol. Sci.*, 2022, **23**, 5687.

41 Z.-Y. Dai, C. Shen, X.-Q. Mi and Q. Pu, *Front. Surg.*, 2023, **10**, 1077492.

42 C. Men, Y. Zhang, P. Shi, Z. Tang and X. Cheng, *Analyst*, 2023, **148**, 6334–6340.

43 E. Cooper, P. J. Choi, W. A. Denny, J. Jose, M. Dragunow and T. I.-H. Park, *Front. Oncol.*, 2021, **11**, 654921.

44 X. Luo, S. Cheng, W. Zhang, K. Dou, R. Wang and F. Yu, *ACS Sens.*, 2024, **9**, 810–819.

45 X. Luo, F. Yu, R. Wang, T. Su, P. Luo, P. Wen and F. Yu, *Chin. Chem. Lett.*, 2025, **36**, 110531.

46 X. Xia, Y. Gai, H. Feng, C. Qin, D. Pan, Y. Song, Y. Zhang and X. Lan, *J. Fluoresc.*, 2020, **30**, 1523–1530.

47 Q. Dou, L. Jiang, D. Kai, C. Owh and X. J. Loh, *Drug Discovery Today*, 2017, **22**, 1400–1411.

48 Z.-Y. Huang, Y.-H. Weng, Y.-F. Yang, B.-H. Lin, Y.-C. Lin and W.-C. Chen, *ACS Photonics*, 2023, **10**, 4509–4518.

49 M. Micheva, S. Baluschev and K. Landfester, *J. Mater. Chem. C*, 2022, **10**, 4533–4545.

50 L. Zeng, L. Huang, J. Han and G. Han, *Acc. Chem. Res.*, 2022, **55**, 2604–2615.

51 S. Askes and S. Bonnet, *Nat. Rev. Chem.*, 2018, **2**, 1.

52 D. K. Mai, C. Kim, J. Lee, T. P. Vales, I. W. Badon, K. De, S. Cho, J. Yang and H.-J. Kim, *Sci. Rep.*, 2022, **12**, 2541.

53 O. Vepris, C. Eich, Y. Feng, H. Zhang, E. Kaijzel and L. Cruz, *Triplet–Triplet Annihilation PLGA-Nanoparticles for Cancer Bioimaging*, 2020.

54 M. A. Walling, J. A. Novak and J. R. E. Shepard, *Int. J. Mol. Sci.*, 2009, **10**, 441–491.

55 M. A. Mimona, M. I. H. Rimon, F. T. Zohura, J. M. Sony, S. I. Rim, M. M. R. Arup and M. H. Mobarak, *Chem. Eng. J. Adv.*, 2025, **21**, 100704.

56 K. Rajamanickam, New Perspectives and Contemporary Applications, in *Quantum Dots - Recent Advances*, IntechOpen, 2022.

57 C. Ge, W. Zhang, J. Huang, B. Qiao, M. Rexiati and A. Zebibula, *Photodiagn. Photodyn. Ther.*, 2025, **52**, 104480.

58 T. A. Henderson and L. D. Morries, *Neuropsychiatr. Dis. Treat.*, 2015, **11**, 2191–2208.

59 B. Chon, W. Ghann, J. Uddin, B. Anvari and V. Kundra, *Int. J. Mol. Sci.*, 2023, **24**, 13030.

60 J. Song, N. Zhang, L. Zhang, H. Yi, Y. Liu, Y. Li, X. Li, M. Wu, L. Hao, Z. Yang and Z. Wang, *Int. J. Nanomed.*, 2019, **14**, 2757–2772.

61 X. Huo, H. Shen, R. Liu and J. Shao, *ACS Omega*, 2021, **6**, 26499–26508.

62 Y. Ma, X. Wang, Z. Wang, G. Zhang, X. Chen, Y. Zhang, Y. Luo, G. Gao and X. Zhou, *Talanta*, 2023, **256**, 124303.

63 J. Cho, F. Nouizi, C.-S. Kim and G. Gulsen, *Sensors*, 2023, **23**, 7728.

64 S. Karma, J. HOMAN, C. Stoianovici and B. Choi, *J. Innovative Opt. Health Sci.*, 2010, **3**, 40–153.

65 D. Su, C. L. Teoh, N. Gao, Q.-H. Xu and Y.-T. Chang, *Sensors*, 2016, **16**, 1397.

66 H. C. Kim and W. H. Park, *Int. J. Biol. Macromol.*, 2019, **135**, 1217–1221.

67 J. Jaklová Dytrtová, K. Moslova, M. Jakl, H. Sirén and M.-L. Riekkola, *Monatsh. Chem.*, 2021, **152**, 1299–1306.

68 C. Deka, B. E. Lehnert, N. M. Lehnert, G. M. Jones, L. A. Sklar and J. A. Steinkamp, *Cytometry*, 1996, **25**, 271–279.

69 M. W. Forbes and R. A. Jockusch, *J. Am. Soc. Mass Spectrom.*, 2011, **22**, 93–109.

70 H. Battula, S. Reddy Bollareddy, V. Vamsi Krishna Venuganti and S. Jayanty, *ChemistrySelect*, 2024, **9**, e202302367.

71 A. S. Kristoffersen, S. R. Erga, B. Hamre and Ø. Frette, *J. Fluoresc.*, 2014, **24**, 1015–1024.

72 R. F. Kubin and A. N. Fletcher, *J. Lumin.*, 1982, **27**, 455–462.

73 Q. Gu, T. M. Sivanandam and C. A. Kim, *Proteome Sci.*, 2006, **4**, 21.

74 G. Wang, M. Zannikou, L. Lofchy, Y. Li, H. Gaikwad, I. V. Balyasnikova and D. Simberg, *ACS Nano*, 2021, **15**, 11880–11890.

75 J. Kang, S. Lhee, J. K. Lee, R. Zare and H. Nam, *Sci. Rep.*, 2020, **10**, 16859.

76 J. Malicka, I. Gryczynski, J. Fang and J. R. Lakowicz, *Anal. Biochem.*, 2003, **317**, 136–146.

77 J. Gottwald, J. Balke, J. Stellmacher, K. van Vorst, F. Ghazisaeedi, M. Fulde and U. Alexiev, *Macromol. Biosci.*, 2024, **24**, 2300437.

78 C. Gebhardt, M. Lehmann, M. M. Reif, M. Zacharias, G. Gemmecker and T. Cordes, *ChemPhysChem*, 2021, **22**, 1566–1583.

79 T. Toyota, H. Fujito, A. Suganami, T. Ouchi, A. Ooishi, A. Aoki, K. Onoue, Y. Muraki, T. Madono, M. Fujinami, Y. Tamura and H. Hayashi, *Bioorg. Med. Chem.*, 2014, **22**, 721–727.

80 A. Gerega, N. Zolek, T. Soltysinski, D. Milej, P. Sawosz, B. Toczylowska and A. Liebert, *J. Biomed. Opt.*, 2011, **16**, 067010.

81 T. Jin, S. Tsuboi, A. Komatsuzaki, Y. Imamura, Y. Muranaka, T. Sakata and H. Yasuda, *Med. Chem. Commun.*, 2016, **7**, 623–631.

82 N. Boens, V. Leen and W. Dehaen, *Chem. Soc. Rev.*, 2012, **41**, 1130–1172.

83 M. Bacalum, L. Wang, S. Boodts, P. Yuan, V. Leen, N. Smisdom, E. Fron, S. Knippenberg, G. Fabre, P. Trouillas, D. Beljonne, W. Dehaen, N. Boens and M. Ameloot, *Langmuir*, 2016, **32**, 3495–3505.

84 X.-F. Zhang and J. Zhu, *J. Lumin.*, 2019, **205**, 148–157.

85 W. Krzemien, M. Rohlickova, M. Machacek, V. Novakova, J. Piskorz and P. Zimcik, *Molecules*, 2021, **26**, 4194.

86 S. Zhu, J. Zhang, G. Vegesna, F.-T. Luo, S. A. Green and H. Liu, *Org. Lett.*, 2011, **13**, 438–441.

87 M. Nakashima, K. Iizuka, M. Karasawa, K. Ishii and Y. Kubo, *J. Mater. Chem. C*, 2018, **6**, 6208–6215.

88 D. Li, P. Jing, L. Sun, Y. An, X. Shan, X. Lu, D. Zhou, D. Han, D. Shen, Y. Zhai, S. Qu, R. Zbořil and A. L. Rogach, *Adv. Mater.*, 2018, **30**, 1705913.

89 L. T. Rosenblum, N. Kosaka, M. Mitsunaga, P. L. Choyke and H. Kobayashi, *Contrast Media Mol. Imaging*, 2011, **6**, 148–152.

90 Z. Han, L. Ren, L. Chen, M. Luo, H. Pan, C. Li and J. Chen, *J. Alloys Compd.*, 2017, **699**, 216–221.

91 S. Omelon, J. Georgiou and W. Habraken, *Biochem. Soc. Trans.*, 2016, **44**, 46–49.

92 A. K. Estandarte, S. Botchway, C. Lynch, M. Yusuf and I. Robinson, *Sci. Rep.*, 2016, **6**, 31417.

93 L. C. Crowley, A. P. Scott, B. J. Marfell, J. A. Boughaba, G. Chojnowski and N. J. Waterhouse, *Cold Spring Harb. Protoc.*, 2016, **7**, DOI: 10.1101/pdb.prot087163.

94 M. Nakamura, A. Awaad, K. Hayashi, K. Ochiai and K. Ishimura, *Chem. Mater.*, 2012, **24**, 3772–3779.

95 H. H. Cui, J. G. Valdez, J. A. Steinkamp and H. A. Crissman, *Cytometry, Part A*, 2003, **52A**, 46–55.

96 A. Samanta, B. K. Paul and N. Guchhait, *J. Photochem. Photobiol., B*, 2012, **109**, 58–67.

97 H. Wang, S. Zhang, X. Tian, C. Liu, L. Zhang, W. Hu, Y. Shao and L. Li, *Sci. Rep.*, 2016, **6**, 34367.

98 L. C. Estrada, M. J. Roberti, S. Simoncelli, V. Levi, P. F. Aramendía and O. E. Martínez, *J. Phys. Chem. B*, 2012, **116**, 2306–2313.

99 M. Zhou, C. Zeng, Q. Li, T. Higaki and R. Jin, *Nanomaterials*, 2019, **9**, 933.

100 K. Nienhaus and G. Ulrich Nienhaus, *RSC Chem. Biol.*, 2021, **2**, 796–814.

101 C. L. Walker, K. A. Lukyanov, I. V. Yampolsky, A. S. Mishin, A. S. Bommarius, A. M. Duraj-Thatte, B. Azizi, L. M. Tolbert and K. M. Solntsev, *Curr. Opin. Chem. Biol.*, 2015, **27**, 64–74.

102 N. G. Bozhanova, M. S. Baranov, N. S. Baleeva, A. S. Gavrikov and A. S. Mishin, *Int. J. Mol. Sci.*, 2018, **19**, 3778.

103 A. V. Mamontova, I. D. Solovyev, A. P. Savitsky, A. M. Shakhov, K. A. Lukyanov and A. M. Bogdanov, *Sci. Rep.*, 2018, **8**, 13224.

104 M. Ormö, A. B. Cubitt, K. Kallio, L. A. Gross, R. Y. Tsien and S. J. Remington, *Science*, 1996, **273**, 1392–1395.

105 K. Joron, J. O. Viegas, L. Haas-Neill, S. Bier, P. Drori, S. Dvir, P. S. L. Lim, S. Rauscher, E. Meshorer and E. Lerner, *Nat. Commun.*, 2023, **14**, 4885.

106 R. Feng, G. Li, C.-N. Ko, Z. Zhang, J.-B. Wan and Q.-W. Zhang, *Small Struct.*, 2023, **4**, 2200131.

107 D. Shcherbo, E. Merzlyak, T. Chepurnykh, A. Fradkov, G. Ermakova, E. Solovieva, K. Lukyanov, E. Bogdanova, A. Zaraisky, S. Lukyanov and D. Chudakov, *Nat. Methods*, 2007, **4**, 741–746.

108 D. Shcherbo, I. I. Shemiakina, A. V. Ryabova, K. E. Luker, B. T. Schmidt, E. A. Souslova, T. V. Gorodnicheva, L. Strukova, K. M. Shidlovskiy, O. V. Britanova, A. G. Zaraysky, K. A. Lukyanov, V. B. Loschenov, G. D. Luker and D. M. Chudakov, *Nat. Methods*, 2010, **7**, 827–829.

109 J. Wei, X. Guo, Y. Wang, Y. Zhang, W. Zhao, S. Han, C. Liu, X. Yang and W. Liang, *Front. Med.*, 2024, **11**, 1461520.

110 X. Luo, E. Hu, F. Deng, C. Zhang and Y. Xian, *Chem. Sci.*, 2025, **16**(15), 6507–6514.

111 A. L. Williams, A. V. Scorzo, R. R. Strawbridge, S. C. Davis and M. Niedre, *JBO*, 2024, **29**, 065003.

112 Y. Hama, Y. Urano, Y. Koyama, M. Kamiya, M. Bernardo, R. S. Paik, I. S. Shin, C. H. Paik, P. L. Choyke and H. Kobayashi, *Cancer Res.*, 2007, **67**, 2791–2799.

113 X. Wang, P. Song, L. Peng, A. Tong and Y. Xiang, *ACS Appl. Mater. Interfaces*, 2016, **8**, 609–616.

114 M. Ulusoy, R. Jonczyk, J.-G. Walter, S. Springer, A. Lavrentieva, F. Stahl, M. Green and T. Scheper, *Bioconjugate Chem.*, 2016, **27**, 414–426.

115 E. Secret, M. Maynadier, A. Gallud, A. Chaix, E. Bouffard, M. Gary-Bobo, N. Marcotte, O. Mongin, K. El Cheikh, V. Hugues, M. Auffan, C. Frochot, A. Morère, P. Maillard, M. Blanchard-Desce, M. J. Sailor, M. Garcia, J.-O. Durand and F. Cunin, *Adv. Mater.*, 2014, **26**, 7643–7648.

116 M. Tasso, M. K. Singh, E. Giovanelli, A. Fragola, V. Loriette, M. Regairaz, F. Dautry, F. Treussart, Z. Lenkei, N. Lequeux and T. Pons, *ACS Appl. Mater. Interfaces*, 2015, **7**, 26904–26913.

117 D. Ag, R. Bongartz, L. E. Dogan, M. Seleci, J.-G. Walter, D. O. Demirkol, F. Stahl, S. Ozcelik, S. Timur and T. Scheper, *Colloids Surf., B*, 2014, **114**, 96–103.

118 Y. Liang, Y. Liu, S. Li, B. Lu, C. Liu, H. Yang, X. Ren and Y. Hou, *Opt. Mater.*, 2019, **89**, 92–99.

119 J. D. Pajović, R. Dojčilović, D. K. Božanić, S. Kaščáková, M. Réfrégiers, S. Dimitrijević-Branković, V. V. Vodnik, A. R. Milosavljević, E. Piscopiello, A. S. Luyt and V. Djoković, *Colloids Surf., B*, 2015, **135**, 742–750.

120 L. Sampath, S. Kwon, M. A. Hall, R. E. Price and E. M. Sevick-Muraca, *Transl. Oncol.*, 2010, **3**, 307–IN1.

121 M. A. Hall, S. Kwon, H. Robinson, P.-A. Lachance, A. Azhdarinia, R. Ranganathan, R. E. Price, W. Chan and E. M. Sevick-Muraca, *Prostate*, 2012, **72**, 129–146.

122 J. Yang, B. Zhu, J. Zhang, S. H. Liang, S. Shen and C. Ran, *Angew. Chem.*, 2024, **136**, e202409896.

123 Z. Duan, Y. Zhu, Y. Yang, Z. He, J. Liu, P. Li, H. Wang and B. Tang, *ChemistryOpen*, 2019, **8**, 316–320.

124 B. Zhou, B. Wang, M. Bai, M. Dong and X. Tang, *Spectrochim. Acta, Part A*, 2023, **294**, 122523.

125 A. V. Scorzo, C. Y. Kwon, R. R. Strawbridge, R. B. Duke, K. L. Chen, C. Li, X. Fan, P. J. Hoopes, D. W. Roberts, K. D. Paulsen and S. C. Davis, *JBO*, 2024, **30**, S13704.

126 M. Hora, I. Trávníček, Š. Nykodýmová, J. Ferda, D. Kacerovská, K. Michalová, O. Hes and S. Minhas, *Contrast Media Mol. Imaging*, 2021, **2021**, 5575730.

127 M. J. Kwon, B. J. House, C. W. Barth, A. Solanki, J. A. Jones, S. C. Davis and S. L. Gibbs, *J. Biomed. Opt.*, 2023, **28**, 082806.

128 N. P. Withana, T. Saito, X. Ma, M. Garland, C. Liu, H. Kosuge, M. Amsallem, M. Verdoes, L. O. Ofori, M. Fischbein, M. Arakawa, Z. Cheng, M. V. McConnell and M. Bogyo, *J. Nucl. Med.*, 2016, **57**, 1583–1590.

129 J. G. de Wit, J. Vonk, F. J. Voskuil, S. A. H. J. de Visscher, K.-P. Schepman, W. T. R. Hooghiemstra, M. D. Linssen, S. G. Elias, G. B. Halmos, B. E. C. Plaat, J. J. Doff, E. L. Rosenthal, D. Robinson, B. van der Vegt, W. B. Nagengast, G. M. van Dam and M. J. H. Witjes, *Nat. Commun.*, 2023, **14**, 4952.

130 A. Watermann, R. Gieringer, A.-M. Bauer, S. Kurch, R. Kiesslich, W. Tremel, J. Gosepath and J. Brieger, *Nanomaterials*, 2019, **9**, 1378.

131 K. E. Wilson, S. V. Bachawal and J. K. Willmann, *Clin. Cancer Res.*, 2018, **24**, 3572–3582.

132 M. Zhang, Q. Zhou, C. Huang, C. T. Chan, W. Wu, G. Li, M. Lim, S. S. Gambhir and H. E. Daldrup-Link, *Mol. Imaging Biol.*, 2022, **24**, 280–287.

133 B. Liu, X. Li, Z. Liu, B. He, H. Xu, J. Cao, F. Zeng, H. Feng, Y. Ren, H. Li, T. Wang, J. Li, Y. Ye, L. Zhao, C. Ran and Y. Li, *J. Med. Chem.*, 2024, **67**, 9104–9123.

134 J. Feng, W. Yang, H. Qin, J. Xu, S. Liu, J. Han, N. Li, L. He and H. Wang, *Front. Pediatr.*, 2023, **11**, 1108997.

135 Y. J. Cho, J.-M. Namgoong, H. H. Kwon, Y. J. Kwon, D. Y. Kim and S. C. Kim, *Front. Pediatr.*, 2021, **9**, 635394.

136 W. S. Yun, H. Cho, S. I. Jeon, D.-K. Lim and K. Kim, *Biomolecules*, 2023, **13**, 1787.

137 R. Giorgio, T. Antonio, B. Gianluca, L. de'Angelis Gian, G. Federica, D. M. Francesco, C. Fausto and D. V. Raffaele, *Acta Biomed.*, 2018, **89**, 135–140.

138 M. Heilemann, in *Comprehensive Biophysics*, ed. E. H. Egelman, Elsevier, Amsterdam, 2012, pp. 39–58.

139 P. He, H. Tang, Y. Zheng, X. Xu, X. Peng, T. Jiang, Y. Xiong, Y. Zhang, Y. Zhang and G. Liu, *Theranostics*, 2025, **15**, 1017–1034.

140 S. Martinelli, L. Fortuna, F. Coratti, F. Passagnoli, A. Amedei and F. Cianchi, *Cancers*, 2024, **16**, 4141.

141 M. Smits, D. Dippel, G. Haan, H. Dekker, P. Vos, D. Kool, P. J. Nederkoorn, P. Hofman, A. Twijnstra, H. Tanghe and M. Hunink, *Radiology*, 2008, **245**, 831–838.

142 F. Dip, E. Lo Menzo, M. Bouvet, R. M. Schols, D. Sherwinter, S. D. Wexner, K. P. White and R. J. Rosenthal, *Surgery*, 2022, **172**, S54–S59.

143 S. H. Emile, H. Elfeki, M. Shalaby, A. Sakr, P. Sileri, S. Laurberg and S. D. Wexner, *J. Surg. Oncol.*, 2017, **116**, 730–740.

144 M. Kapoor, T. F. Heston and A. Kasi, in *StatPearls*, StatPearls Publishing, Treasure Island (FL), 2025.

145 J. Trotter, A. R. Pantel, B.-K. K. Teo, F. E. Escorcia, T. Li, D. A. Pryma and N. K. Taunk, *Adv. Radiat. Oncol.*, 2023, **8**, 101212.

146 J. Rong, A. Haider, T. E. Jeppesen, L. Josephson and S. H. Liang, *Nat. Commun.*, 2023, **14**, 3257.

147 R. Massari and G. S. P. Mok, *Front. Med.*, 2023, **10**, 1349877.

148 Y. Bouchareb, A. AlSaadi, J. Zabah, A. Jain, A. Al-Jabri, P. Phiri, J. Q. Shi, G. Delanerolle and S. R. Sirasanagandla, *Diagnostics*, 2024, **14**, 1431.

149 S. Yandrapalli and Y. Puckett, in *StatPearls*, StatPearls Publishing, Treasure Island (FL), 2025.

150 D. L. Bailey and K. P. Willowson, *J. Nucl. Med.*, 2013, **54**, 83–89.

151 S. R. Cherry, T. Jones, J. S. Karp, J. Qi, W. W. Moses and R. D. Badawi, *J. Nucl. Med.*, 2018, **59**, 3–12.

152 M. Al Moudi, Z. Sun and N. Lenzo, *Biomed. Imaging Intervention J.*, 2011, **7**, e9.

153 R. J. Palyo, A. J. Sinusas and Y.-H. Liu, *J. Nucl. Med.*, 2016, **57**, 893–899.

154 M. E. Phelps, *Proc. Natl. Acad. Sci. U. S. A.*, 2000, **97**, 9226–9233.

155 S. Vandenberghe, P. Moskal and J. S. Karp, *EJNMMI Phys.*, 2020, **7**, 35.

156 J. Rao, A. Dragulescu-Andrasi and H. Yao, *Curr. Opin. Biotechnol.*, 2007, **18**, 17–25.

157 J. Kasem, U. Wazir and K. Mokbel, *In Vivo*, 2021, **35**, 23–30.

158 B. Huang, M. Bates and X. Zhuang, *Annu. Rev. Biochem.*, 2009, **78**, 993–1016.

159 J. Chojnacki and C. Eggeling, *Retrovirology*, 2018, **15**, 41.

160 T. Watakabe, R. Toya, T. Saito, T. Matsuyama, S. Shiraishi, Y. Kai, Y. Shimohigashi and N. Oya, *Anticancer Res.*, 2020, **40**, 2567–2572.

161 M. Ljungberg and P. H. Pretorius, *Br. J. Radiol.*, 2018, **91**, 20160402.

162 Z. Cheng, P. Chen and J. Yan, *EJNMMI Phys.*, 2025, **12**, 9.

163 F.-M. Lu and Z. Yuan, *Quant. Imaging Med. Surg.*, 2015, **5**, 433–447.

164 Z. J. Wang, T.-T. A. Chang and R. Slauter, in *A Comprehensive Guide to Toxicology in Nonclinical Drug Development*, ed. A. S. Faqi, Academic Press, Boston, 2nd edn, 2017, pp. 921–938.

165 J. M. Quesada-Olarte, M. E. Allaf, M. Alvarez-Maestro and L. Martínez-Piñeiroa, *Actas Urol. Esp.*, 2020, **44**, 386–399.

166 J. C. Waters, *J. Cell Biol.*, 2009, **185**, 1135–1148.

167 S. A. Haider, A. Cameron, P. Siva, D. Lui, M. J. Shafiee, A. Boroomand, N. Haider and A. Wong, *Sci. Rep.*, 2016, **6**, 20640.

168 W. A. McDougald and J. G. Mannheim, *EJNMMI Phys.*, 2022, **9**, 77.

169 H. Iida, T. Zeniya, M. Yamauchi, K. Koshino, T. Temma, S. Iguchi, M. Yamazaki, J. Enmi, N. Kondo, N. Motomura and J. Nakagawara, in *Perspectives on Nuclear Medicine for Molecular Diagnosis and Integrated Therapy*, ed. Y. Kuge, T. Shiga and N. Tamaki, Springer Japan, Tokyo, 2016, pp. 17–38.

170 N. Rathod, W. Jutidamrongphan, W. A. Bosbach, Y. Chen, J. L. Penner, H. Sari, K. Zeimpekis, A. L. Montes, P. Moskal, E. Stepien, K. Shi, A. Rominger and R. Seifert, *Semin. Nucl. Med.*, 2025, **55**, 98–106.

171 T. Etrych, O. Janoušková and P. Chytil, *Pharmaceutics*, 2019, **11**, 471.

172 S. Bouccara, A. Fragola, E. Giovanelli, G. Sitbon, N. Lequeux, T. Pons and V. Loriette, *J. Biomed. Opt.*, 2014, **19**, 051208.

173 T. Yoshimura, A. Hasegawa, S. Kogame, K. Magota, R. Kimura, S. Watanabe, K. Hirata and H. Sugimori, *Diagnostics*, 2022, **12**, 872.

174 A. Refaat, M. L. Yap, G. Pietersz, A. P. G. Walsh, J. Zeller, B. del Rosal, X. Wang and K. Peter, *J. Nanobiotechnol.*, 2022, **20**, 450.

175 N. Liu, S. He, Z. Cheng and J. Hu, *Coord. Chem. Rev.*, 2025, **532**, 216511.

176 Z. A. Qureshi, H. Dabash, D. Ponnamma and M. K. G. Abbas, *Heliyon*, 2024, **10**, e31634.

177 T. Bhattacharya, G. H. Shin and J. T. Kim, *Pharmaceutics*, 2023, **15**, 1019.

178 H. Bao, Y. Liu, H. Li, W. Qi and K. Sun, *Heliyon*, 2023, **9**, e20317.

179 S. D. Hettiarachchi, R. M. Graham, K. J. Mintz, Y. Zhou, S. Vanni, Z. Peng and R. M. Leblanc, *Nanoscale*, 2019, **11**, 6192–6205.

180 C. E. Tiron, G. Luta, M. Butura, F. Zugun-Eloae, C. S. Stan, A. Coroaba, E.-L. Ursu, G. D. Stanciu and A. Tiron, *Sci. Rep.*, 2020, **10**, 12662.

181 Y. Su, S. Liu, Y. Guan, Z. Xie, M. Zheng and X. Jing, *Biomaterials*, 2020, **255**, 120110.

182 A. K. Mia, M. Meyyappan and P. K. Giri, *Biosensors*, 2023, **13**, 169.

183 C. Wulandari, N. L. W. Septiani, G. Gumilar, Nugraha, H. S. Wasisto and B. Yuliarto, *ChemBioEng Rev.*, 2024, **11**, 278–298.

184 N. Rohaizad, C. C. Mayorga-Martinez, M. Fojtů, N. M. Latiff and M. Pumera, *Chem. Soc. Rev.*, 2021, **50**, 619–657.

185 G. Reina, G. M. Beneventi, R. Kaur, G. Biagiotti, A. Cadranel, C. Ménard-Moyon, Y. Nishina, B. Richichi, D. M. Guldi and A. Bianco, *Chem.–Eur. J.*, 2023, **29**, e202300266.

186 G. Li, C. Chen, Y. Li, B. Wang, J. Wen, M. Guo, M. Chen, X.-B. Zhang and G. Ke, *Nano Lett.*, 2024, **24**, 11335–11348.

187 Z. Hao, L. Kong, L. Ruan and Z. Deng, *Nanomaterials*, 2024, **14**, 1968.

188 Z. He, K. Shi, J. Li and J. Chao, *iScience*, 2023, **26**, 106638.

189 P. Venkatesan, P. Pal, S. S. Ng, J.-Y. Lin and R.-A. Doong, *Coord. Chem. Rev.*, 2025, **523**, 216266.

190 L. Huang and G. Han, *Nat. Rev. Chem.*, 2024, **8**(4), 238–255.

191 C. J. O'Dea, J. Isokuortti, E. E. Comer, S. T. Roberts and Z. A. Page, *ACS Cent. Sci.*, 2024, **10**, 272–282.

192 M. P. Rauch and R. R. Knowles, *Chimia*, 2018, **72**, 501–507.

193 X. Qin, J. Wang and Q. Yuan, *Front. Chem.*, 2020, **8**, 608578.

194 U. Cho and J. K. Chen, *Cell Chem. Biol.*, 2020, **27**, 921–936.

195 L. Ceresa, J. Chavez, E. Kitchner, J. Kimball, I. Gryczynski and Z. Gryczynski, *Exp. Biol. Med.*, 2022, **247**, 1840–1851.

196 R. Ziniuk, A. Yakovliev, J. Qu and T. Ohulchanskyy, *Time-gated and lifetime-unmixed imaging of near- and short wave infrared photoluminescence from rare-earth ion doped nanoparticles*, 2019.

197 D. Jin and J. A. Piper, *Anal. Chem.*, 2011, **83**, 2294–2300.

198 W. Yang and S.-L. Chen, *J. Innovative Opt. Health Sci.*, 2020, **13**(3), 2030006.

199 J. Li, J. Liu, V. Das, H. Le, N. Aguilera, A. J. Bower, J. P. Giannini, R. Lu, S. Abouassali, E. Y. Chew, B. P. Brooks, W. M. Zein, L. A. Huryn, A. Volkov, T. Liu and J. Tam, *Commun. Med.*, 2025, **5**, 1–11.

200 R. Monsour, M. Dutta, A.-Z. Mohamed, A. Borkowski and N. A. Viswanadhan, *Fed. Pract.*, 2022, **39**, S14–S20.

201 D. Hussain and Y. Hyeon Gu, *Diagnostics*, 2024, **14**, 1328.

202 I. R. Nabi, B. Cardoen, I. M. Khater, G. Gao, T. H. Wong and G. Hamarneh, *J. Cell Biol.*, 2024, **223**, e202311073.

203 J. Chojnacki and C. Eggeling, *Retrovirology*, 2018, **15**, 41.

204 K. Prakash, B. Diederich, R. Heintzmann and L. Schermelleh, *Philos. Trans. R. Soc., A*, 2022, **380**, 20210110.

205 C. Rodríguez, S. Arlt, L. Möckl and M. Krenn, *Nat. Commun.*, 2024, **15**, 10658.

206 R. Chen, X. Tang, Y. Zhao, Z. Shen, M. Zhang, Y. Shen, T. Li, C. H. Y. Chung, L. Zhang, J. Wang, B. Cui, P. Fei, Y. Guo, S. Du and S. Yao, *Nat. Commun.*, 2023, **14**, 2854.

207 M. A. Labouesse, R. B. Cola and T. Patriarchi, *Int. J. Mol. Sci.*, 2020, **21**, 8048.

208 T. Patriarchi, A. Mohebi, J. Sun, A. Marley, R. Liang, C. Dong, K. Pugher, G. O. Mizuno, C. M. Davis, B. Wiltgen, M. von Zastrow, J. D. Berke and L. Tian, *Nat. Methods*, 2020, **17**, 1147–1155.

209 E. C. Wright, E. Scott and L. Tian, *Neuropsychopharmacology*, 2025, **50**, 269–273.

210 S. Zuo, Y. Li, T. Ren and L. Yuan, *Sens. Diagn.*, 2024, **3**(1), 28–39.

211 J. R. Benson, F. W. B. van Leeuwen and T. Sugie, *Front. Oncol.*, 2021, **11**, 776832.

212 P. A. Sutton, M. A. van Dam, R. A. Cahill, S. Mieog, K. Polom, A. L. Vahrmeijer and J. van der Vorst, *BJS Open*, 2023, **7**, zrad049.

213 J. T. Alander, I. Kaartinen, A. Laakso, T. Pätilä, T. Spillmann, V. V. Tuchin, M. Venermo and P. Välisuo, *Int. J. Biomed. Imaging*, 2012, **2012**, 940585.

214 S. Zeb, J. E. Villa, A. Wong, S. Khan, S. Hussain and M. Sotomayor, *J. Braz. Chem. Soc.*, 2023, **34**(5), 615–640.

215 N. Rezaei, M. R. Safarnejad, S. Soheilivand, R. H. Sajedi, J. Mahmoudian and M. Shams-Bakhsh, *Physiol. Mol. Plant Pathol.*, 2025, **138**, 102689.